DE GRUYTER OPEN

Acta Geophysica
vol. 64, no. 6, Dec. 2016, pp. 2677-2716
DOI: 10.1515/acgeo-2016-0064

Early Thermal History of Rhea: The Role of Serpentinization and Liquid State Convection

Leszek CZECHOWSKI[1] and Anna ŁOSIAK[2,3]

[1]Institute of Geophysics, Faculty of Physics, University of Warsaw, Warszawa, Poland; e-mail: lczecho@op.pl

[2]Institute of Geological Sciences, Polish Academy of Sciences in Wrocław, Wrocław, Poland

[3]Department of Lithospheric Research, University of Vienna, Vienna, Austria

A b s t r a c t

Early thermal history of Rhea is investigated. The role of the following parameters of the model is investigated: time of beginning of accretion, t_{ini}, duration of accretion, t_{ac}, viscosity of ice close to the melting point, η_0, activation energy in the formula for viscosity, E, thermal conductivity of silicate component, k_{sil}, ammonia content, X_{NH3}, and energy of serpentinization, c_{serp}. We found that t_{ini} and t_{ac} are crucial for evolution. All other parameters are also important, but no dramatic differences are found for realistic values. The process of differentiation is also investigated. It is found that liquid state convection could delay the differentiation for hundreds of My. The results are confronted with observational data from Cassini spacecraft. It is possible that differentiation is fully completed but the density of formed core is close to the mean density. If this interpretation is correct, then Rhea could have accreted any time before 3-4 My after formation of CAI.

Key words: medium-sized satellites, thermal evolution, gravitational differentiation, serpentinization, Rhea.

1. INTRODUCTION

The group of medium-sized icy satellite (MIS) of Saturn consists of 6 bodies. The largest is Rhea with a radius of 764 km, and the smallest is Mimas with a radius of 199 km. All of MIS are spherical bodies. They consist of mixtures of rocks and ices.

The impact craters are the most common structures found on the surface of Rhea (*e.g.*, Plescia 1985, De Pater and Lissauer 2001, p. 203); therefore, it was classified as a dead body by Rothery (1992). However, the Cassini mission revealed presence of younger structures of tectonic and volcanic origin (*e.g.*, Jaumann *et al.* 2009).

For the present research (as well as for Czechowski 2012) the data concerning gravitational field are especially important. Analysis of the Doppler data acquired by the Cassini spacecraft yields the mass of Rhea and the quadrupole moments of its gravity field with high accuracy. Eventually, Iess *et al.* (2007) conclude: "the data exclude fully differentiated models in which the core would be composed of unhydrated silicates and the mantle would be composed of pure ice. […] The one model that fits the gravity data and is self-consistent when energy transport and ice melting are qualitatively considered is an "almost undifferentiated" Rhea, in which a very large uniform core is surrounded by a relatively thin ice shell containing no rock at all". This conclusion gives some bounds for our investigation.

The radar observations of Rhea give information about chemical composition of the surface layer. The layer consists mostly of the water ice surface with organic polymers and carbon dioxide present in small amounts. The ammonia bearing compounds are absent on the surface but radar indicates an increase in ammonia with depth. Anyway, the total content of ammonia in Rhea is probably low (Ostro *et al.* 2006, Prentice 2006).

A few papers considered thermal evolution of Rhea. Summaries of previous investigations of thermal history of Rhea (and other MIS) are given in Schubert *et al.* (2010), Matson *et al.* (2009), and Czechowski (2012). Rhea is probably the best (of all MIS of Saturn) object for modeling because there is no tidal heating. Matson *et al.* (2009) provides a limited information concerning thermal evolution of Rhea; this study stated that the temperature increase due to despinning could be up to ~20 K, and due to accretion ~90 K. Moreover, according to Barr and Canup (2008), Rhea was formed no earlier than 4 My after the CAI (Calcium-Aluminium-rich Inclusions in meteorites) condensation, if Rhea is indeed undifferentiated.

We used numerical methods similar to Czechowski (2012). However, we consider different problems. First, we discuss the role of meteorite data for research concerning Rhea. This part could be used also for other medium-sized icy satellites. Although the role of meteoritic data for models of MIS is

known, it is rarely discussed in details. Second, the role of chemical composition and chemical reactions in Rhea is discussed. This problem has not been considered in Czechowski (2012) at all. Third, we investigate the role of different parameters important for thermal evolution. Moreover, we give more attention to details of the process of differentiation. A better model of grains' sinking is presented. Finally, the role of serpentinization for thermal evolution is calculated. To our best knowledge, it is the first thermal model of Rhea where serpentinization is included.

The paper is organized as follows. MIS and the basic properties of meteorite material are discussed in Section 2. Section 3 discusses heat sources and general properties of convection. The numerical model of heat transfer used for our calculations is presented in Section 4. The thermal history and the role of different parameters are discussed in Section 5. Conclusions are in the last section.

2. MATERIAL PROPERTIES OF MIS

2.1 Differentiation of the MIS

MIS consist of two types of materials characterized by very different physical properties: ices of volatiles (mostly H_2O with a small addition of CO_2 and NH_3) and a silicate-metal mixture. The average density of the icy component is relatively well constrained and varies within a narrow range of 930-1010 kg m^{-3}. The pressure in the center of Rhea is below 200 MPa, so only ices Ic, Ih, and (below temperature ~75 K) I XI are possible (see Fig. 1). Their densities are ~940 kg m^{-3} (Cogoni *et al.* 2011).

Densities used to represent the rocky component of MIS vary significantly, from 2500 kg m^{-3} (Schubert *et al.* 2007), through 2700 kg m^{-3} (Porco *et al.* 2006), up to as much as 3250 kg m^{-3} (Prialnik and Merk 2008) or even 3500 kg m^{-3} (Schubert *et al.* 2007, 2010). However, those highest values are not in agreement with the current understanding of the process of the formation and evolution of icy satellites (*e.g.*, Castillo-Rogez *et al.* 2007, Schubert *et al.* 2007, Zolotov 2007, Sohl *et al.* 2010).

The icy satellites of the giant planets are thought to be mostly formed by aggregation of thermally unprocessed, aqueously unaltered dust particles from the solar accretion disk (Canup and Ward 2009, Mosqueira *et al.* 2010, Coradini *et al.* 2010, Sohl *et al.* 2010). However, some addition of material by collisions with planetesimals is also possible (*e.g.*, Kargel *et al.* 2000). The constituents of the icy satellites' rocky fraction were anhydrous and reduced at the time of formation. They consisted mostly of Fe-Ni metal, FeS, Mg-, and Ca-silicates, Ca-Al oxides and organic matter. The initial chemical composition of the silicate phase was probably similar to either carbona-

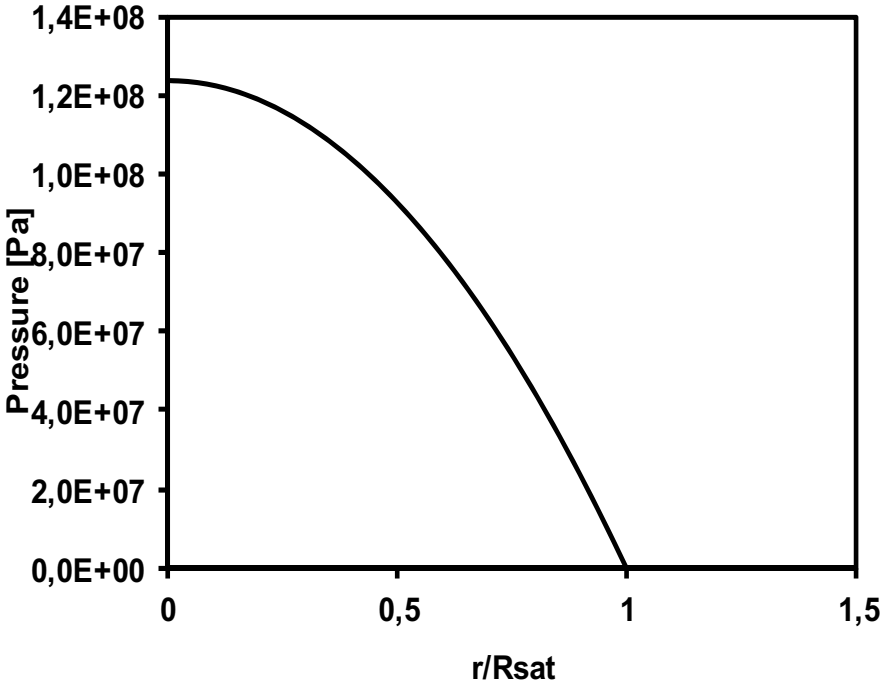

Fig. 1. Pressure distribution in Rhea. Note that the pressure in the center is below 200 MPa, so only ices Ic, Ih, and I XI are possible (Cogoni *et al.* 2011).

ceous chondrites (Kargel *et al.* 2000, Zolotov and Shock 2001, McKinnon and Zolensky 2003) or L/LL chondrites (Kuskov and Kronrod 2005).

After accretion, energy from the decay of radionuclides increased temperature of the satellites. Since most of radionuclides were enclosed within the silicate grains, the rocky particles were behaving as local heat sources and could melt the adhering ices. The first melts could have been formed under relatively low temperatures (Sohl *et al.* 2010) if the water ice was contaminated; *e.g.*, an eutectic brine of NH_3-H_2O can form at 175 K (Desch *et al.* 2009) and HCl hydrates melt at 186 K (Zolotov and Mironenko 2007). With the increase of temperature, the size of melt pockets increases and the liquid composition became more diluted (Zolotov and Mironenko 2007). The other possible sources of energy are: gravitational energy from silicate-ice differentiation (core forming), gravitational energy from contraction, kinetic energy from impacts, mineral hydration reactions, and tidal energy (*e.g.*, Schubert *et al.* 2007, Hussmann *et al.* 2010). For MIS, the energy of differentiation is not important. Moreover for Rhea the tidal energy is probably not important either (unless Rhea was in an orbit-orbit resonance in the

past). The energy of impacts heats only upper layers, so its role for global processes is rather limited, except in a case of very catastrophic impacts.

If temperature was high for a long enough time, then melt pockets formed around silicate grains converged. If, moreover, the liquid volume is significant (~50%) then silicate grains are moving towards the center of mass forming a differentiated body with a rocky core and icy mantle (*e.g.*, Schubert *et al.* 2007, Sohl *et al.* 2010, Travis *et al.* 2012). If the temperature did not reach the melting temperature, the satellite remained undifferentiated. In the case of differentiated bodies, the temperature could continue to increase. If it approached 775-875 K, previously hydrated minerals started to disintegrate and their bounded water was removed from the mineral structure (*e.g.*, Peacock 2001, Llana-Funez *et al.* 2007), although subsequent hydration, after dropping the temperature, is very probable, especially since dehydration increases porosity (*e.g.*, Rutter *et al.* 2009). If the temperature rose to more than approximately 1275 K, the silicate-metal core could have differentiated (*e.g.*, Showman and Malhotra 1999, Sohl *et al.* 2002, Schubert *et al.* 2010). This situation probably has not occurred in MIS.

2.2 Post-differentiation hydrothermal activity

The rock-water interaction continued also after the process of MIS body differentiation was completed because the silicate cores were permeable and in contact with the ocean. Terrestrial rocks are permeable up to the pressure of 300 MPa (Walsh and Brice 1984); the permeability is probably of the order of $\sim 10^{-17}$ m^2 (*e.g.*, Stein *et al.* 1995, Sinha and Evans 2004, Sohl *et al.* 2010). It means that even large icy satellites (such as Europa) have probably 20-30 km thick layer of upper rocky core permeable for water.

In smaller bodies (such as Rhea), the pressure and its gradient are low; therefore, the entire silicate core should be permeable for water (Fig. 1). It means that if the lower part of the volatile-rich mantle is melted (forming an underground ocean at the core-mantle boundary) then the silicate-water interaction could continue after core formation (Sohl *et al.* 2010). This could have led to the formation of extensive hydrothermal circulation system within MIS bodies (Travis *et al.* 2012) that would influence the thermal history of Rhea by enabling serpentanization to occur over long time periods. The duration of extensive hydrothermal circulation depends on many factors. Note that the permeability could decrease as a result of a high pressure gradient and crystallization of secondary minerals within pores. These processes and the cooling of the satellite could reduce the Rayleigh number below its critical value (*e.g.*, Czechowski and Kossacki 2012). In the largest icy satellites such as Titan, Ganymede and Triton, the silicate-water interaction could

have been limited by the formation of high pressure ices on the bottom of the sea (Sohl *et al.* 2010).

The two most important consequences of the water-rock interaction are: (i) dissolution of water-soluble elements in the liquid phase which significantly decreases freezing temperature, and (ii) formation of hydrated and oxidized minerals which replace anhydrous particles (*e.g.*, Hutchison 2004, Weisberg *et al.* 2006, Brearley 2006, Bland *et al.* 2009). Hydration of minerals can significantly change their physical properties, *e.g.*, it decreases the average density of material: during oxidation, metallic Fe (~7500 kg m^{-3}) transforms to much less dense magnetite (5120 kg m^{-3}), and hydration of olivine (3300 kg m^{-3}) leads to the formation of serpentine (~2500 kg m^{-3}). Additionally, the serpentinization process can serve as an additional source of heat which can be a driving force of the hydrothermal systems, especially in the later stages of satellite evolution (Vance *et al.* 2007).

The interaction of the rocky and icy phases based on the model described above is consistent not only with the thermochemical equilibria models (*e.g.*, Zolotov 2007), but also with (i) the analogue studies on meteorites from hydrated parent bodies (Brearley 2006), (ii) terrestrial low temperature weathering on Antarctica (Jull *et al.* 1988, Velbel *et al.* 1991, Losiak and Velbel 2011), (iii) the direct Cassini observations of the properties of water vapor plume and ice particles emerging from Enceladus (*e.g.*, Postberg *et al.* 2011), and (iv) the discovery of multiple non-icy materials (abundant hydrated sulfates: $MgSO_4 * nH_2O$, $Na_2SO_4 * nH_2O$, and $H_2SO_4*nH_2O$) on the surface of icy Galilean satellites of Jupiter (Dalton *et al.* 2005).

2.3 Meteorite properties

Remote sensing and numerical modeling show that non-volatile component of MIS has the same composition as hydrated chondritic meteorites (*e.g.*, Kargel *et al.* 2000, Zolotov and Shock 2001, McKinnon and Zolensky 2003, Kuskov and Kronrod 2005) such as Ivuna-type carbonaceous chondrite (CI) and Mighei-type carbonaceous chondrite (CM) (*e.g.*, Brearley 2006, Bland *et al.* 2009). All of the CI and CM meteorites, including those that were collected immediately after their fall on Earth, are extensively aqueously altered (*e.g.*, Hutchison 2004). Aqueous alteration resulted in the partial (CMs) or complete (CIs) disintegration of the chondrules, and formation of a phyllosilicate matrix. The contents of the bound (structural) water within those carbonaceous chondrites can be up to 22% (*e.g.*, Hutchison 2004, Weisberg *et al.* 2006).

The process of aqueous alteration on the CI and CM parent bodies occurred in relatively static water with ices constituting about 50% of volume (*e.g.*, Young *et al.* 2003); the metasomatic elemental fractionation occurred

only over very short distances (*e.g.*, Young *et al.* 2003, Brearley 2004, 2006; Rubin *et al.* 2007, Bland *et al.* 2009). This statement is based on survival of highly water-reactive phases until terrestrial exposure (*e.g.*, Jull *et al.* 1988, Gounelle and Zolensky 2001, Losiak and Velbel 2011), and the fact that water-soluble element abundances are nearly uniform in bulk samples of all CMs. In the case of CM meteorites, the extent of silicate hydration was limited by the water availability (Velbel *et al.* 2012), while in the icy satellites the hydration was probably more restricted by the temperature.

The CI chondrites' matrix consists of serpentine interlayered with saponite and other phases embedded within them, such as magnetite, sulfides (pyrrhotite, pentlandite, cubanite), carbonates (calcite, dolomite, beunnerite, siderite), and sulfates (gypsum, epsomite, bloedite, Ni bloedite) (*e.g.*, Tomeoka and Buseck 1988, Brearley 2006). The measurements of physical properties of CI meteorites are rarely undertaken because they are: (i) very rare (only 5 separate falls are known), (ii) very valuable because of their pristine chemical composition, and (iii) extremely fragile. The Orgueil CI chondrite from the Vatican collection has a grain density of 2430 kg m^{-3} and a bulk density of 1580 kg m^{-3} (with porosity of 35%) (Consolmagno and Britt 1998, Macke *et al.* 2011). No data on the thermal conductivity of the CI meteorites is available.

The CM meteorites are less aqueously altered than CIs; they still have recognizable chondrules (about 20% of volume), calcium-aluminum-rich inclusions (about 5%) and even some remnants of metal grains (Brearley and Jones 1998). However, they are mainly composed of the matrix rich in phyllosilicates and other aqueously altered phases such as magnetite, various sulfides, sulfates, carbonates, halides (halite and sylvite), hydroxides (brucite) as well as silicates such as chlorite saponite and vermiculite (*e.g.*, Brearley 2006, Velbel *et al.* 2012). Since CMs are much more abundant, more measurements are available. The average grain density is 2920 kg m^{-3} (min 2740 kg m^{-3} and max 3260 kg m^{-3}) (Macke *et al.* 2011). The average bulk density of the CM type is 2200 kg m^{-3} (from 1880 kg m^{-3} to 2470 kg m^{-3}) (Macke *et al.* 2011), although it can be as low as 1662 kg m^{-3} (Opeil *et al.* 2010). The average porosity of CM chondrites is around 24.7% (from 15.0% to 36.7%.) (Macke *et al.* 2011). The thermal conductivity of the CM2 meteorite (Cold Bokkeveld, density 1662 kg m^{-3}) measured at 200 K is very low: 0.5 W m^{-1} K^{-1}, specific heat c_p = 500 J kg^{-1} K^{-1}, thermal diffusivity κ = 6.02×10^{7} m^2 s^{-1} and inverse thermal inertia $\Gamma = 15.51\times10^{4}$ m^2 $s^{1/2}$ kJ^{-1} (Opeil *et al.* 2010). The thermal conductivity k for the range of temperature between 6 K and 300 K increases with temperature and can be approximated by the equation (Opeil *et al.* 2010):

$$k = -0.0254 + 0.00563T - 2.07\times10^{-5}\,T^2 + 3.11\times10^{-8}\,T^3 .$$

Low values of thermal conductivity of those meteorites are mainly a result of their high porosity and bad contact between the grains. In MIS the pressure is higher, then the contact is better and possible pores are filled with ice (or water), that significantly changes the bulk conductivity. Therefore, we mainly used data for grains instead of the bulk values for porous meteorites.

3. HEAT SOURCES AND GENERAL PROPERTIES OF CONVECTION

3.1 Heat sources

Endogenic activity needs a source of heat. In the present paper we consider the following heat sources: decay of SLI (Short-Lived radioactive Isotopes, *i.e.*, Al^{26}, Fe^{60}, Mn^{53}), decay of LLI (Long-Lived radioactive Isotopes, *i.e.*, K^{40}, Th^{232}, U^{238}, U^{235}), the heat of serpentinization, and the heat of accretion (*e.g.*, Prialnik *et al.* 1987). The initial heat rates generated by a given isotope just after formation of CAI are given in Table 1. For any given time t the heat rate per 1 kg is:

$$Q(t) = f_m \sum_{i=1}^{7} Q_{oi} \exp\left(-C_i t\right), \tag{1}$$

where f_m is a silicate mass fraction in the medium and time t is measured from the formation of CAI. Other symbols are explained in Table 1.

It is known that the tidal heating is an important source of heat in some satellites (*e.g.*, Czechowski 2006, Castillo-Rogez 2006) but for Rhea it could be neglected, because the tidal parameter ψ for Rhea is low; ψ is defined as:

Table 1

Data concerning radioactive isotopes considered in the paper
(after Robuchon *et al.* 2010, modified)

Isotope	Half life $t_{1/2}$ [My]	Initial rate of heating per unit mass of element [W kg^{-1}]	Isotopic concentration *ppb* [10^{-9}]	Half life $t_{1/2}$ [s]	Decay constant C_i [s^{-1}]	Initial rate of heating per unit mass of silicate Q_{0i} [W kg^{-1}]
U238	4468	9.47E-05	26.2	1.409E+17	4.916E-18	2.48E-12
U235	703.81	5.69E-04	8.2	2.221E+16	3.120E-17	4.66E-12
Th232	14030	2.64E-05	53.8	4.427E+17	1.565E-18	1.42E-12
K40	1277	2.92E-05	1104	4.029E+16	1.720E-17	3.22E-11
AL28	0.716	3.41E-01	600	2.259E+13	3.067E-14	2.05E-07
Fe60	1.5	7.10E-02	200	4.733E+13	1.464E-14	1.42E-08
Mn53	3.7	2.70E-02	25.7	1.167E+14	5.936E-15	6.94E-10

$$\psi = M R_{\rm sat}{}^3/(m a^3)\,, \tag{2}$$

where $R_{\rm sat}$ is the radius of satellite, m is its mass, M is the mass of Saturn, and a is the semimajor axis of the satellite orbit. For Rhea $\psi = 0.000748$ only. For more details, see discussion in Czechowski (2012).

The heat of accretion results from kinetic energy of the accreting matter. The temperature of an accreting layer $T_{\rm ac}$ could be calculated from the formula (*e.g.*, Multhaup and Spohn 2007):

$$T_{\rm ac} = (4/3\ c_{\rm p})\ \xi\ \pi\ G\ \rho\ R^2(t)\ (1 + 1/2e) + T_{\rm nebula}\,, \tag{3}$$

where $G = 6.67\ 10^{-11}$ N m^2 kg^{-2} is the gravity constant, ρ is the density, $R(t)$ is the current radius of the accreting body, c_p is the specific heat. We adopt also here constant $\xi = 0.4$ and the Safronov number $e = 2$ after Multhaup and Spohn (2007). The initial distribution of the temperature in our models is calculated using Eq. 3. The surface temperature on Rhea and the nebula temperature are assumed to be the same, namely $T_{\rm s} = T_{\rm nebula} = 75$ K. This is a typical value used in similar models (*e.g.*, Multhaup and Spohn 2007). It corresponds approximately to the present surface temperature of the Saturnian satellites. Some models use higher temperature of the nebula (*e.g.*, 250 K – see Multhaup and Spohn 2007). However, such high initial temperature of interior of Rhea could be presently excluded from the consideration because it leads to widespread melting and differentiation of the interior. The observation of Iess *et al.* (2007) suggests very limited differentiation only.

According to the considerations from previous section and discussion in Sections 2.1-2.3, we included the reaction of serpentinization as a source of heat. After Abramov and Mojzsis (2011) we consider the following reaction:

$$Mg_2SiO_4\ (\text{forsterite}) + MgSiO_3\ (\text{enstatite}) + 2H_2O \dashrightarrow Mg_3Si_2O_5(OH)_4\ (\text{antigorite}) \tag{4}$$

This reaction releases ~240 000 J per kg of serpentine produced (~69 kJ per mole). Similar reactions were considered by Malamud and Prialnik (2013). We are interested mainly in energy released during serpentinization; therefore, we do not discuss details of these chemical processes. The density of serpentine is 2470 kg m^{-3} but we assume that the silicates contain also 20% of nonreactive rock of density 3630 kg m^{-3} (Abramov and Mojzsis 2011). Although many values of density are used in models of MIS (see discussion in Section 2.1) we eventually have chosen the silicate density according to Abramov and Mojzsis (2011), *i.e.*, 2470 × 80% + 3630 × 20% = 2702 kg m^{-3} and 240 000 J kg^{-1} for energy of serpentinization.

Table 2

Basic data and formulae used in the considered model

Symbol	Formula or value	Remarks	Reference
R_{Sat} [m]	764 300	Final radius of Rhea	Iess *et al.* (2007)
$R(t)$ [m]	$R(t) = A\ t$ for $t_{ini} < t < t_{ini} + t_{ac}$	Radius of Rhea during accretion	
ρ_{ice} [kg m^{-3}]	940	Density of ice	Iess *et al.* (2007)
ρ_{sil} [kg m^{-3}]	2470 80% + 3630 20%= 2702	Density of silicates	See text
ρ [kg m^{-3}]	1233	Density of Rhea	Iess *et al.* (2007)
f_V [1]	$f_V = (\rho - \rho_{ice})/(\rho_{sil} - \rho_{ice})$	Volume fraction of silicates	
f_m [1]	$f_m = \rho_{sil} f_V / \rho$	Mass fraction of silicates	
k_{ice} [W m^{-1} K^{-1}]	$0.4685 + 488.12/T$	Thermal conductivity of ice	Robuchon *et al.* (2010)
k_{sil} [W m^{-1} K^{-1}]	4.2 or 2.5	Thermal conductivity of silicates	See text
k [W m^{-1} K^{-1}]	$f_v\ k_{sil} + (1 - f_v)\ k_{ice}$	Thermal conductivity	
$c_{p\,ice}$ [J kg^{-1} K^{-1}]	$185 + 7.037\ T$	Specific heat of ice	Castillo-Rogez *et al.* (2007)
$c_{p\,sil}$ [J kg^{-1} K^{-1}]	920	Specific heat of silicates	Castillo-Rogez *et al.* (2007)
c_p [J kg^{-1} K^{-1}]	$f_m\ c_{sil} + (1 - f_m)\ c_{ice}$	Specific heat	
c_{serp} [J kg^{-1}]	241 000	Heat of serpentinization	Abramov and Mojzsis (2011)
$c_{p\,melts}$ [J kg^{-1}K^{-1}]	4180	Specific heat of water	
c_m [J kg^{-1}]	333×10^3	Latent heat of melting of ice	
T_m [K]	$273.15 - 7.95\times10^{-8}\ p - 9.6\times10^{-17}\ p^2 - 0.538\ X_{NH3} - 6.5\times10^{2}\ X_{NH3}{}^2 - 4.4\times10^{8}\ p\ X_{NH3}$	Temperature of melting (p is the pressure, X_{NH3} is the content of ammonia)	Leliwa-Kopystynski *et al.* (2002)
α [K^{-1}]	1.56×10^{-4}	Coefficient of thermal expansion	Hobbs (1974)
$g(r)$ [m s^{-2}]	$(4/3)\ \pi\ G\ \rho\ r$	Gravity at given r	
D [m]		Thickness of the considered spherical layer	

3.2 Solid state convection

Following Czechowski (2012) two types of large-scale motion in Rhea interior are considered in the present paper: solid state thermal convection (SSC) and thermal convection in liquid (LSC – Liquid State Convection). The SSC is a very slow convection observed in media that are solid (from microscopic point of view) but behave like liquid in specific conditions. Interiors of many planets and satellites could be treated as liquid in geological time. Some global tectonic structures on MIS could be interpreted as results of solid-state convection (*e.g.*, Czechowski and Leliwa-Kopystyński 2003, Schubert *et al.* 1986, Kargel and Pozio 1996). The very large values of the Prandtl number *Pr* are characteristic for this motion. *Pr* is defined as:

$$Pr = \eta / \rho \kappa , \tag{5}$$

where η [Pa s] denotes the effective viscosity, κ [m^2 s^{-1}] is the thermal diffusivity, and ρ [kg m^{-3}] is the density. For solid state convection in Rhea $Pr = O(10^{20})$. It means that inertial terms in the equation of motion could be neglected (*e.g.*, Czechowski 1993).

The Rayleigh number *Ra* is used to characterize the intensity of convection. The intensity increases with *Ra*. The exact form of *Ra* depends on a specific physical situation. In situations considered here the heating for SSC is mainly from below, because the liquid water (in the core) is below its lower boundary, so the lower boundary could be treated as isothermal. Therefore, for SSC we use the following definition of the Rayleigh number *Ra* (*e.g.*, Schubert *et al.* 2001, p. 270):

$$Ra = \rho g_r \alpha \Delta T d^3 / (\kappa \eta) , \tag{6}$$

where g_r is the average gravity in the considered region [m s^{-2}], α is the coefficient of thermal volume expansion [K^{-1}], $\kappa = k/(\rho c_p)$ is the coefficient of temperature diffusion where c_p is the specific heat [J kg^{-1}K^{-1}], k is the thermal conductivity [W m^{-1} K^{-1}], ΔT is the temperature difference [K] across the considered region (layer), d is the thickness of this layer, and $\eta(T)$ is the effective (temperature dependent) viscosity [Pa s]. The $\eta(T)$ is evaluated for the average temperature T_{av} in the considered region (similar symbol T_{ave} is used here for the average temperature of the whole satellite). Other non-constant parameters (*e.g.*, κ, ρ) are also averaged over the considered region. The temperature difference $\Delta T = T_{\mathrm{m}} - T_s$, where T_s is the surface temperature and T_{m} is the temperature of the molten region. If there is no melted core at all, then temperature in the center T_c is used instead of T_{m}. Convection starts if the Rayleigh number exceeds its critical value Ra_{cr}. Value of Ra_{cr} depends on the situation, but usually $Ra_{\mathrm{cr}} = O(1000)$, (*e.g.*, Turcotte and Schubert 2002), so we choose $Ra_{\mathrm{cr}} = 1000$. Note that sometimes *Ra* is de-

fined in a different way; our value of Ra_{cr} corresponds to Ra defined using $\eta(T)$ evaluated for the average temperature T_{av} in the considered region (*e.g.*, Czechowski 1993, p. 221).

3.3 Liquid state convection

The second mode of thermal convection considered here (LSC) could take place in a molten region. The Prandtl number is $Pr = O(1)$. It means that inertial forces like Coriolis force could be important for this motion (*e.g.*, Czechowski 2012).

In the molten region the viscosity drops several orders, even down to $\eta = O(10^{-3})$ Pa s. It means that Ra increases several orders, up to 10^{14} or even more. The LSC could be very intensive, resulting in almost adiabatic temperature gradient. So in the molten core we assume the adiabatic gradient expressed by:

$$\frac{dT}{dr} = \frac{g\alpha_w T}{c_{pw}}, \tag{7}$$

where r is the radial distance (spherical coordinate), α_w is the thermal expansion coefficient, and c_{pw} is the specific heat for liquid water, g is the gravity in the core. Equation 7 indicates very low temperature gradient. Note also that coefficient of thermal expansion α_w of water is negative for $T < 277$ K at low and moderate pressures. For pressure corresponding to the central part of Rhea the anomaly of α_w disappears and $\alpha_w > 0$. For outer parts of Rhea, LSC requires temperature higher than 277 K. The serpentinization (starting after melting) could be a source of additional heat that leads to fast increase of the temperature of the molten region, up to $T > 277$ K, making the LSC possible just after the melting (without the need for the increase of temperature resulting from the radiogenic heating).

Czechowski (2014) indicates that velocity of LSC could be higher than the terminal velocity of typical grains (diameter ~1 mm) even in small Enceladus. The terminal velocity v_{term} is the velocity of a sinking grain where gravity is compensated by other forces. In Rhea, the velocity of LSC could be higher than in Enceladus. It means that (for some time) the mixing prevails over differentiation. The differentiation could occur only when LSC is slowing down (see Section 5.3 below). It means that for most of the time, LSC is getting heat from the inside (the grains with radioactive isotopes are suspended in the liquid), so we use Ra_{in} defined for internal heating as follows:

$$Ra_{in} = \alpha_m \rho_m^2 g d^5 Q(t)/(k_m \kappa_m \eta_m), \tag{8}$$

where subscript m denotes that given parameter is calculated for molten region of the satellite. Note that liquid water contains suspended solids, so the values of these parameters are not the same as for the water. The $\kappa_m = k_m / (\rho_m\, c_{pm})$ is the average value of coefficient of temperature diffusion, and k_m is average thermal conductivity [W m^{-1} K^{-1}], and $Q(t)$ is the rate of heating per 1 kg.

3.4 Viscosity of the solid mantle

The volume percentage of rocky component in Rhea is approximately ~17%. It means that rheological properties of its interior are determined by the icy component (Roscoe 1952, Schubert *et al.* 1986). According to Mangold *et al.* (2002) the creep is observed for the content of ice above 28%. However, for small content of the ice the viscosity is 10 to 50 times higher than for pure ice.

In general, the uppermost layer of the satellite ("lithosphere") is elastic for small deformation and brittle for large deformations. The medium below the lithosphere is also solid but for very slow geologic processes it behaves like a viscous fluid. There are no observational data concerning temperature-dependent viscosity $\eta(T)$ of the interior of MIS. Therefore, we should investigate the problem for some range of viscosity. After Czechowski (2012) we started from the formula:

$$\eta(T) = \eta_x\ \sigma^{(1-i)}\ \exp\left(\frac{E}{RT}\right), \tag{9}$$

where η_x is a constant, σ is the second invariant of the deviatoric stress tensor, i is the power law index ($i = 1$ corresponds to a Newtonian fluid), E is the activation energy of the dominant mechanism of deformation, and $R = 8.314$ [J K^{-1} mole^{-1}] is the universal gas constant (McKinnon 1998, Goldsby and Kohlstedt 1997, Durham *et al.* 1998, Forni *et al.* 1991). Parameters η_x, E and i depend on many factors; *e.g.*, size of ice crystal, content of gases, size of mineral grains *etc*., most of them being essentially unknown. Durham *et al.* (1998) give two extreme values of E: 43 kJ mole^{-1} (for water ice I below 195 K) and 107.5 kJ mole^{-1} (for NH_3*$2H_2O$). These values correspond to E/R: 5172 K and 12 930 K, respectively. Rheology of both materials is highly nonlinear. Fortunately, non-Newtonian flow could be simulated by Newtonian flow with lower E (Christensen 1984, Dumoulin *et al.* 1999); therefore, we assume that $i = 1$ (*i.e.*, Newtonian flow) but we use $E = 50$ kJ kg^{-1} mole^{-1}.

The viscosity η_0 for the melting temperature T_m is used as a parameter in our model. It is equal to:

$$\eta_0 = \eta(T_m) = \eta_x \exp\left(\frac{E}{R\,T_m}\right). \tag{10}$$

However, we use here some results of Solomatov (1995) for the temperature-dependent viscosity convection. He considers the viscosity in the form:

$$\eta(T) = \eta_S \exp\left(-\gamma\, T\right), \tag{11}$$

where η_S and γ are constants (see also: Davaille and Jaupart 1993, Grasset and Parmentier 1998). To achieve the compatibility of Eqs. 9 and 11, we introduce:

$$\gamma = E/(R\,\zeta^2\,T_m^{\,2}), \tag{12}$$

where ζ is a parameter ($0 < \zeta \leq 1$) and T_m denotes the melting temperature. The constant η_S is given by:

$$\eta_S = \eta_0 \exp\left[E\,(2/\zeta - 1)/R\,T_m\right]. \tag{13}$$

For such η_S, Eqs. 9 and 11 give the same value of viscosity for $T = T_m$ and $\varsigma = 1$, $i = 1$.

4. NUMERICAL MODEL

4.1 Basic equations of the model

The parameterized theory of convection used in Czechowski (2012) is chosen for the present research. It is based on the 1-dimensional equation of the heat transfer in spherical coordinates:

$$\rho\, c_p \frac{\partial T(r,t)}{\partial t} = \mathrm{div}(\,k(r,T)\,\mathrm{grad}\,T(r,t)) + q(r,T,t)\,, \tag{14}$$

where r is the radial distance (spherical coordinate), ρ is the density [kg m^{-3}], c_p [J kg^1 K^{-1}] is the specific heat, $q(r, T, t) = \rho\, Q$ [W m^{-3}] is the heat rate per unit volume, and k [W m^{-1} K^{-1}] is the thermal conductivity. Note that $Q(r, t)$ includes sources and sinks of the heat: radiogenic heat resulting from the decay of isotopes, latent heat of melting and latent heat of solidification. The heat of accretion is used to calculated temperature of the accreting material (see Eq. 3). This temperature is used as the boundary condition for temperature during accretion.

If the Rayleigh number in the considered layer exceeds its critical value Ra_{cr}, then the convection starts (*e.g.*, Czechowski 1993, p. 180; Czechowski and Kossacki 2009). The effect of convection can be described by dimensionless Nusselt number Nu (*e.g.*, Sharpe and Peltier 1978, Peltier and Jarvis 1982, Czechowski 2006, compare also Davies 2007). We use the following

definition of *Nu* (*e.g.*, Czechowski 1993, p. 185; Czechowski and Kossacki 2012):

$$Nu = (\text{True total surface heat flow}) / (\text{Total heat flow without convection}) . \quad (15)$$

Now one can include the heat transport by convection simply multiplying the k in the considered spherical region:

$$k_{\text{conv}} = Nu\, k , \quad (16)$$

where k_{conv} is an effective coefficient of the heat conduction. Of course, the temperature distribution obtained from 1D parameterized theory is different comparing to the true 3 D distribution. Fortunately, the details of temperature distribution are not important for our calculations. It is enough that the average temperature of the layer and total heat transfer through the layer will correspond to the true ones. This condition is satisfied.

For the Nusselt number, Czechowski (2012) uses formulae given by Solomatov (1995) for temperature-dependent viscosity. Solomatov (1995) considered 3 cases: the low viscosity contrast between hot interior and cold upper part of the convective layer, the medium viscosity contrast, and the high viscosity contrast. However, our preliminary calculations have shown that a simpler approach is satisfactory. Therefore, after Turcotte and Schubert (2002, p. 273) we use:

$$Nu = 1.04\, (Ra / Ra_{\text{crit}})^{1/3} . \quad (17)$$

Equation 14 is solved for $R(t) \geq r \geq 0$, where $R(t)$ is the current radius of Rhea. During accretion the radius $R(t)$ increases in time, namely: $R(t) = A\, t$ (where A is a constant) for $t_{\text{ini}} < t < t_{\text{ini}} + t_{\text{ac}}$. The constant A is chosen in such a way that $R(t) = R_{Sat} = 763$ km for $t = t_{\text{ini}} + t_{\text{ac}}$, *i.e.*, when accretion is completed. The linear function chosen for $R(t)$ means that the rate of mass accretion is increasing as $R(t)^3$ that agrees with the increasing geometrical and gravitational cross-sections of the accreting body. The linear function is also used by Merk *et al.* (2002). The temperature of accreted matter depends on the radius $R(t)$ (and consequently on the mass) of the proto-Rhea and is given by Eq. 3.

5. ROLE OF PARAMETERS FOR THERMAL EVOLUTION

5.1 Temperature limit

The upper limit for the temperature (*i.e.*, the potential temperature) inside Rhea can be calculated neglecting the heat transport. Graphs of the potential temperature (both upper lines) and potential melting (lower lines) for Rhea versus time of start of accretion t_{ini} (counted from forming CAI) are given in Fig. 2. There are included: the heat production from the radioactive decay during 20 My (after time t_{ini}), the heat of serpentinization (if melting has oc-

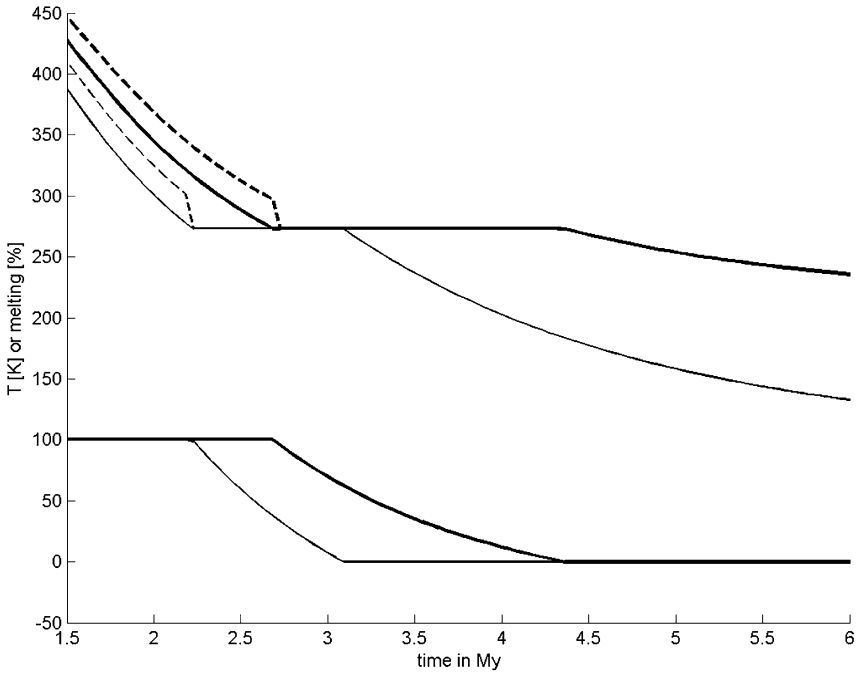

Fig. 2. Graphs of potential temperature (the solid and dashed upper lines) and potential melting (lower solid lines) for Rhea versus time of the beginning of accretion $t_{\rm ini}$. The dashed lines give results for total heat of radioactive decay during 20 My (after time $t_{\rm ini}$) and serpentinization. The thick lines included also the heat of accretion. The heat transfer is neglected so all heat is used for temperature increase and melting. The solid lines are for heating without serpentinization. The effect of serpentinization is seen as sharp steps on the upper lines. The value of 100% for lower lines (presenting potential melting) means that total latent heat of ice melting is supplied.

curred) and the heat of accretion. All heat is used for the temperature increase and/or melting (note that melting occurs only if the latent heat of melting is transferred to the medium). The solid lines give results for radiogenic heat and serpentinization. The dotted line is for heating without serpentinization. For early accretion (*i.e.*, t_{ini} =1 My) the maximum temperature is ~500 K. For more realistic t_{ini} = 2 My, the upper limit for T is ~400 K. The effect of serpentinization is seen as the sharp steps on the plots of temperatures (upper solid lines). The release of chemical energy is possible only in the molten medium. If heat of accretion is negligible then for $t_{ini} > 2.2$ My melting is not possible as well as differentiation and serpentinization. Therefore, the dashed lines representing temperature without serpentinization are below the solid lines. Note also that the temperature of accreting material

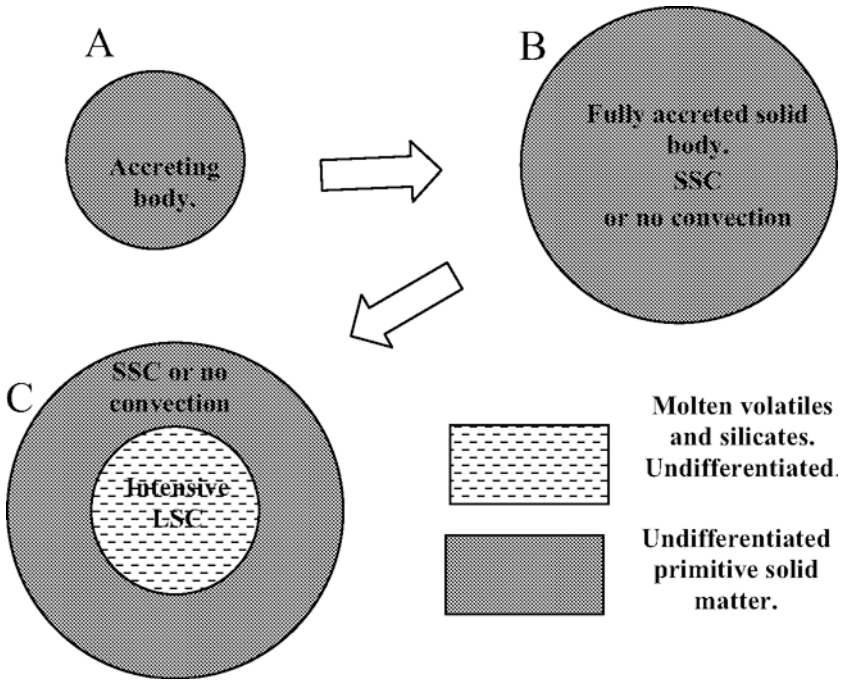

Fig. 3. Scheme of the considered evolution: A − accreting body, B − fully accreted solid body, C − if heating from SLI is intensive enough then part of the body is melted forming two layers body (melted: "core" and solid: "mantle"). After Czechowski (2012), modified.

(calculated according to Eq. 3) depends on the current radius of the body during accretion. Therefore, two cases are presented: for the center of the satellite (no heat of accretion – thick lines) and for the surface (where maximum of energy is released – thin lines). If the heat of accretion is included then melting (as well as differentiation and serpentinization) is possible even for t_{ini}~2.7 My.

The scheme of the considered evolution is given in Fig. 3. We start from accretion (Fig. 3A). The accreting body is solid, with initially inverse temperature gradient (*i.e.*, $\partial T/\partial r > 0$). The fully accreted solid body is also initially solid, but the negative temperature gradient is established in a few My, so SSC is possible for most of the time (Fig. 3B). The stage of evolution presented in Fig. 3C is reached only if heating from SLI is intensive enough to melt part of the satellite. Then two layers are formed, melted central sphere referred here as a "core" and solid layer referred here as a "mantle". In the

core one could expect intensive LSC. SSC could operate in the solid mantle. The scheme is rather simple but interactions of the processes give quite complicated possible evolutionary paths, which are discussed below.

5.2 Role of model's parameters

The values of the most important parameters of our model are not known with a good accuracy. Therefore, we investigate thermal history of Rhea for different values of them to determine the role of each parameter. The role of following parameters is considered: time of beginning of accretion, t_{ini} , viscosity of ice close to the melting point, η_0, activation energy in the formula for viscosity, E, duration of accretion, t_{ac}, energy of serpentinization, c_{serp}, and content of ammonia, X_{NH3}. Figures 4-9 present evolution of globally averaged temperature T_{ave} (weighted average) and temperature in the center of the body T_c. T_{ave} and T_{c} represent the thermal state of Rhea and therefore are the best for our purpose. Horizontal axis gives $\log_{10}(t)$, where t is the time from CAI formation in My.

Figure 4 gives results for the following set of values of parameters: $\eta_0 = 10^{14}$ Pa s, E = 50 kJ kg^{-1} mole^{-1}, t_{ac}=0.1 My, c_{serp} = 240 000 J kg^{-1}, X_{NH3} = 0, k_{sil} = 4.2 Wm^{-1} K^{-1}. Moreover, 3 values of time of the beginning of accretion t_{ini} are used: 1.2, 2.4, and 4.2 My. These values will be referred here as the "basic" values and the model that uses them as the basic model. Comparing to Czechowski (2012) we use different values of t_{ini}, t_{ac} and η_0. The increase of η_0 is based on the results of Mangold *et al.* (2002) discussed in Section 3.4. We try also shorter t_{ac} = 0.1 My (it is justified by the results of Mosqueira *et al.* 2010, Merk *et al.* 2002). Later accretion characterized by larger t_{ini} is a consequence of shorter t_{ac}. Note that low t_{ini} means a large degree of differentiation.

Consider now the case for t_{ini}=1.2 My. The model is simple but one can see a few stages of evolution. They are (all given times are counted from the formation of CAI):

- From 1.2 to 1.3 My − accretion. In this case (short duration of accretion, t_{ac} = 0.1 My) the inverse gradient of temperature (*i.e.*, $\partial T/\partial r > 0$) is maintained to the end of accretion; consequently, SSC is not possible.
- From 1.3 to 2 My. SLI and LLI have supplied enough heat for establishing normal temperature gradient (*i.e.*, $\partial T/\partial r < 0$). It leads to an outburst of very intensive SSC (like an overturn, $Ra \approx 10^7\, Ra_{cr}$). Large loss of the heat results in substantial decreases of T_{ave}. This intensive SSC lasts from ~1.3 to ~1.9 My. During this time the centre of Rhea reaches the melting temperature. The latent heat stabilizes the temperature of the center T_{c} from ~1.5 to ~2 My.

- From 2 to 2.1 My − rapid increase of the molten region. The thickness of the solid "mantle" decreases from 100% of the radius of Rhea R_{sat} down to ~21% of R_{sat}. This results in a large decrease of intensity of SSC (see Eq. 6).
- From 2.1 to 7 My. Intensive SSC in the solid "mantle" with $Ra \approx 10^4 Ra_{cr}$ and intensive LSC in the molten "core" are developed. LSC maintains an adiabatic gradient of the temperature in the "core". The velocity of LSC is high and consequently LSC does not allow differentiation of the melted region. The thickness of the solid mantle decreases down to ~14% of R_{sat}. Maxima of T_c and T_{ave} are reached at ~7 My.
- From 7 to 400 My. In general, very slow cooling but the thickness of the solid mantle is still decreasing down to ~7% of R_{sat} at 70 My. The intensity of both LSC and SSC decreases because radiogenic heating by SLI is decreasing. However, even for 400 My (the end of our modeling) both modes of convection operate and the radius of molten region is still ~78% of R_{sat}.

Consider now the case t_{ini} = 2.4 My. SLI have supplied enough heat for establishing the normal temperature gradient (*i.e.*, $\partial T/\partial r < 0$) at ~2.7 My and SSC starts and its intensity increases. The maximum value of $Ra \approx 10^6 Ra_{cr}$ is reached at 5 My. However, there is no rapid outburst and there is no temporary decrease of T_{ave}. The maximum of T_{ave} is reached at t = 3.2 My. It is followed by slow decreasing of Ra and T_{ave}. T_c reaches T_m at 4.2 My and stabilizes to 220 My. Eventually no part of satellite is melted and the stage C from Fig. 3 is never reached. Also there is no heating from serpentinization. After 220 My, T_c starts to decrease.

Consider now the case t_{ini} = 4.2 My. The role of SSC is moderate for thermal evolution. SSC starts at 5.4 My and its intensity increases very slowly. Maximum $Ra \approx 10^2 Ra_{cr}$ is reached at 120 My. T_c reaches its maximum at 200 My.

Concluding, results for the "basic" model indicate the crucial role of t_{ini} for evolution. The melting, differentiation and forming core are possible only for the low value of t_{ini} (see also Fig. 3). The final (*i.e.*, at ~400 My) thermal states of models without melting (*i.e.*, here for t_{ini} = 2.4 and 4.2 My) are essentially the same because they differ only in the initial heat input. The final state of models with melting is not the same, because of different thermal properties of core, different distribution of LSI, *etc*.

Compare now models with different values of chosen parameters. The role of η_0 is presented in Fig. 5. The value of η_0 is increased from "basic" 10^{14} to 10^{16} Pa s. Graphs of two models are plotted together; the thinner lines are for the basic model and thick lines are for model with $\eta_0 = 10^{16}$ Pa s. Higher η_0 means lower Ra and consequently decreased efficiency of cooling.

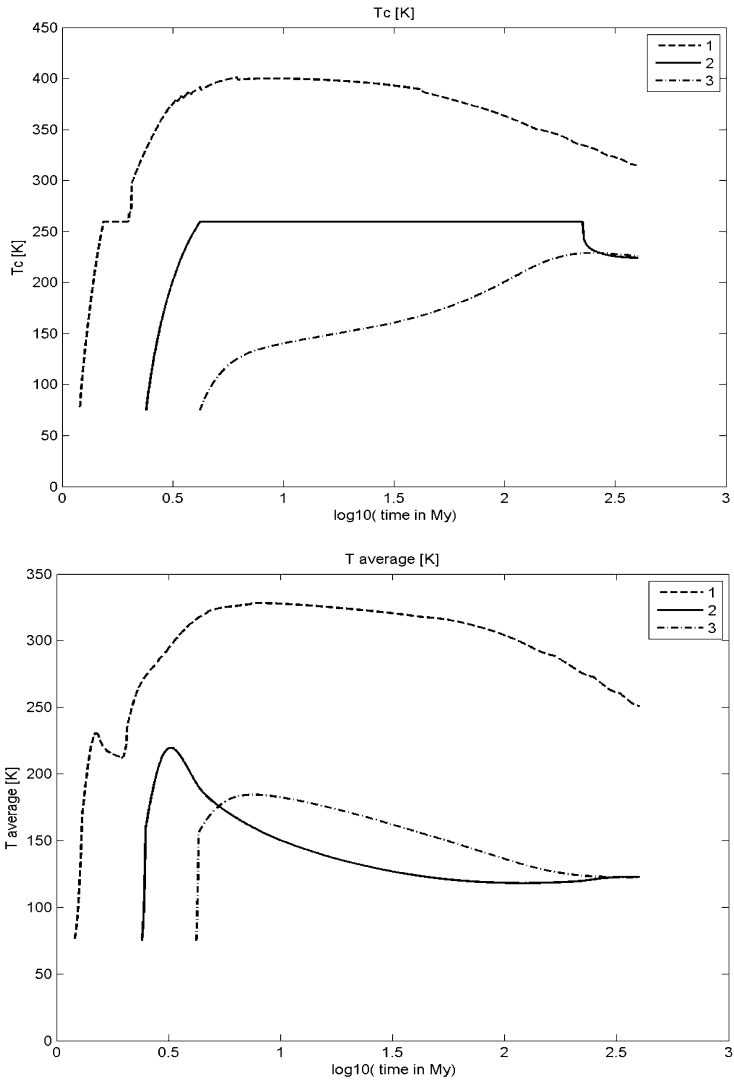

Fig. 4. The results for the "basic" model, *i.e.*, for the following values of parameters: viscosity parameter $\eta_0 = 10^{14}$ Pa s, the activation energy $E = 5\times10^4$ J mole^{-1}, the duration of accretion $t_{ac} = 0.1$ My, the energy for serpentinization $c_{serp} = 240\ 000$ J kg^{-1}, and the ammonia content $X_{NH3} = 0$. The upper panel presents the evolution of temperature in the center of the satellite T_c *versus* time t. The lower panel presents average temperature of the satellite T_{ave}. Horizontal axis gives $\log_{10}(t)$, where t is time from CAI formation in My. Evolutions for 3 different times of beginning of accretion t_{ini} are given. Lines from the left to the right correspond to: $t_{ini} = 1.2$ My (dashed line 1), 2.4 My (solid line 2), 4.2 My (dashed-dotted line 3), respectively. More explanation in the text.

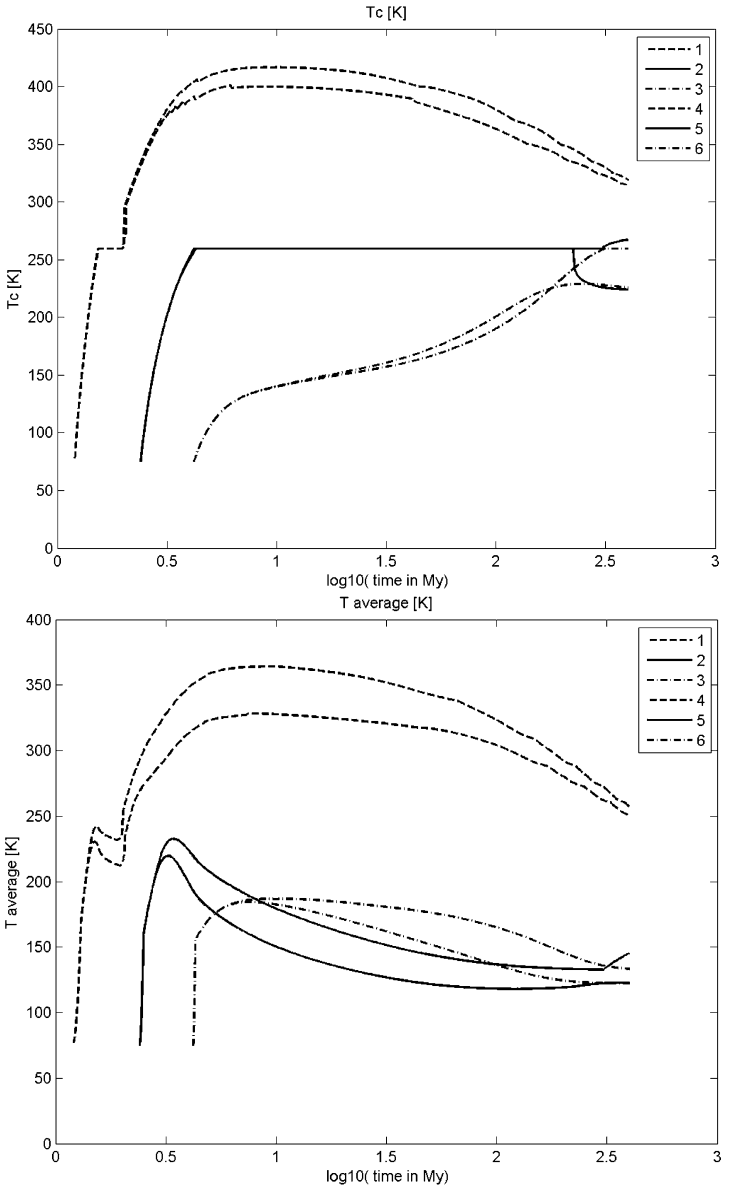

Fig. 5. The role of viscosity η_0 for thermal evolution. Two values of η_0 are used: 10^{14} Pa s (thin lines) and 10^{16} Pa s (thick lines). The higher value of η_0 reduces the role of SSC in the solid part of the satellite. The rest of parameters have the "basic" values, *i.e.*, $t_{ac} = 0.1$ My, $c_{serp} = 240\,000$ J kg^{-1}, and $E = 5\times10^4$ J mole^{-1}, $k_{sil} = 4.2$ W m^{-1} K^{-1}, $X_{NH3} = 0$. Lines from the left to the right correspond to $t_{ini} = 1.2$ My (dashed lines: 1 and 4), 2.4 My (solid lines: 2 and 5), 4.2 My (dashed-dotted lines: 3 and 6), respectively.

Therefore, generally temperatures for the "basic" model are below temperatures for $\eta_0 = 10^{16}$. Note also that for $\eta_0 = 10^{16}$, for the case of $t_{ini} = 2.4$ My (thick solid line in the upper panel) temperature in the center T_c exceeded melting temperature after ~380 My. This is possible because some heat from accretion released in upper layers is conducted to the center of the satellite (compare discussion in Section 5.1 and Fig. 2). Melting means also a release of serpentinization energy. Eventually both, T_c and T_{ave}, increase after ~380 My.

The case for $t_{ini} = 4.2$ My in Fig. 5 is interesting because the lines for the basic model are (for some time) slightly above lines for $\eta_0 = 10^{16}$ Pa s. Such nonlinear effects are common for evolution determined by SSC. Later, the lines intersect at ~180 My and eventually lines for basic model merge with the lines for $t_{ini} = 2.4$ My. The merging is expected because for 400 My SLI virtually does not exist and SSC is very weak. Therefore, the final thermal state of undifferentiated Rhea is determined by LLI and thermal conductivity only.

The role of energy of activation E is presented in Fig. 6. The value of E is decreased from the "basic" 5×10^4 J mole^{-1} to 3×10^4 J mole^{-1}. Lower E means lower viscosity. It increases Ra and consequently increases the efficiency of cooling; therefore, lines for the 'basic' model are generally above the lines for $E = 3\ 10^4$. Note a substantial difference of evolution of T_c for $t_{ini} = 2.4$ My (thick solid line in the upper panel) comparing to the basic model (thin solid line in the upper panel); the duration when $T_c = T_m$ is much shorter comparing to the basic model. For $t_{ini} = 4.2$ My both lines intersect similarly to the case presented in Fig. 5.

Figure 7 presents effects of longer duration of accretion t_{ac}. The longer t_{ac} means that more energy of accretion and radiogenic energy is lost because of small size of accreting body. For $t_{ini} = 1.2$ the effect is very substantial; T_c and T_{ave} are lower on ~100 K for ~300 My. It is also a result of SSC in accreting body (SSC starts at 1.5 My, *i.e.*, 0.3 My after start of accretion). For $t_{ini} = 2.4$ My the effect is weaker; SSC starts at 3.1 My, T_{ave} is lower on ~50K for a few My, the duration of $T_c = T_m$ is much shorter (the solid lines in the upper panel of Fig. 7). For $t_{ini} = 4.2$ My the effect is even weaker but still visible.

The role of energy of serpentinization c_{serp} for thermal evolution is given in Fig. 8. Two values of c_{serp} are used: 0 J kg^{-1} (thick lines) and the "basic" value 240 000 J kg^{-1} (thin lines). The effect is possible only if serpentinization have occurred, *i.e.*, if some part of the Rhea is melted. Therefore, the temperature drop on ~20 K is observed only for $t_{ini} = 1.2$ My.

Figure 9 presents the role of ammonia content X_{NH3}. Two values of X_{NH3} are used: $X_{NH3} = 0.1$ (thick lines) and $X_{NH3} = 0$ (thin lines). The main effect of NH_3 is a decrease of the melting temperature T_m (see Table 2). For

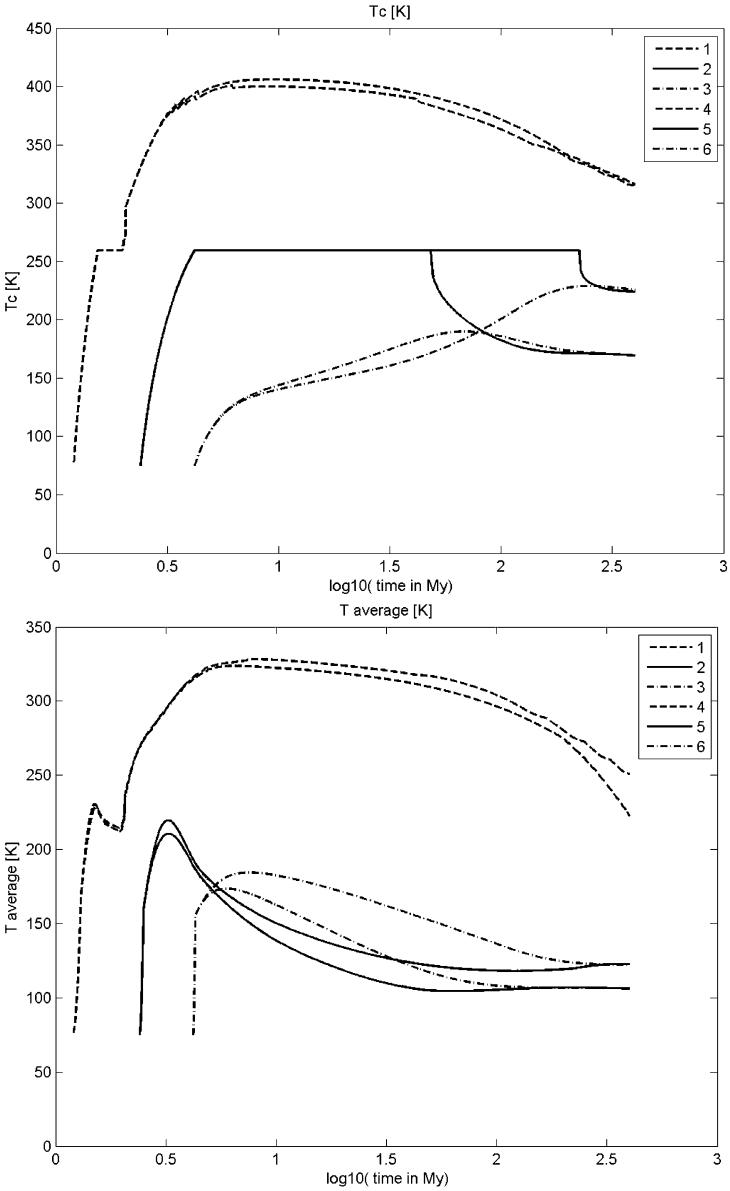

Fig. 6. The role of activation energy E for thermal evolution. Two values of activation energy are used: $E = 3\times10^4$ J mole^{-1} (thick lines) and $E = 5\times10^4$ J mole^{-1} (thin lines). The lower value of E increases the cooling effect of SSC in the solid part of the satellite. The rest of parameters have the "basic" values, *i.e.*, $t_{ac} = 0.1$ My, $\eta_0 = 10^{14}$ Pa s, $c_{serp} = 240\,000$ J kg^{-1}, $k_{sil} = 4.2$ W m^{-1} K^{-1}, $X_{NH3} = 0$. Lines from the left to the right correspond to $t_{ini} = 1.2$ My (dashed lines: 1 and 4), 2.4 My (solid lines: 2 and 5), 4.2 My (dashed-dotted lines: 3 and 6), respectively.

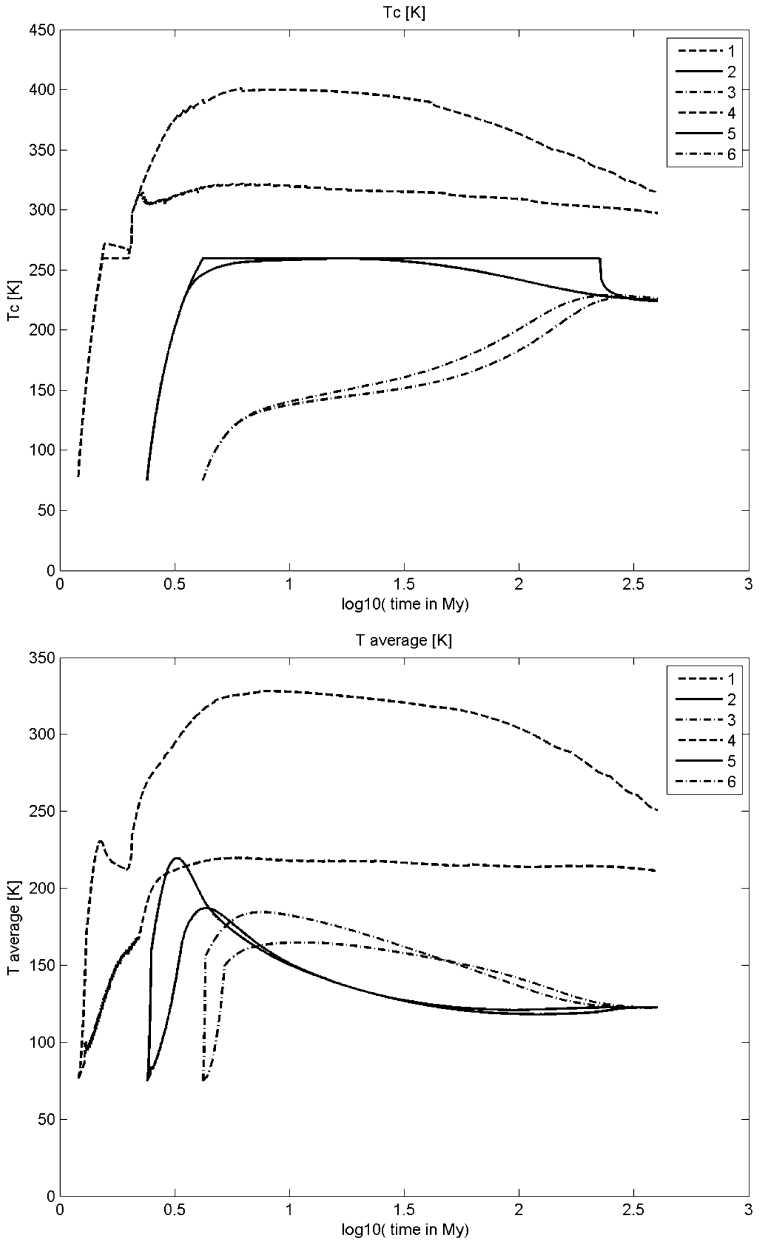

Fig. 7. The role of duration of accretion t_{ac} for thermal evolution. Two values of t_{ac} are used: $t_{ac} = 1$ My (thick lines) and $t_{ac} = 0.1$ My (thin lines). Lines from the left to the right correspond to $t_{ini} = 1.2$, 2.4, 4.2 My, respectively. The increased value of t_{ac} generally decreases temperature. The role of t_{ac} is similar to role of time of beginning of convection t_{ini}. The rest of parameters have their "basic" values.

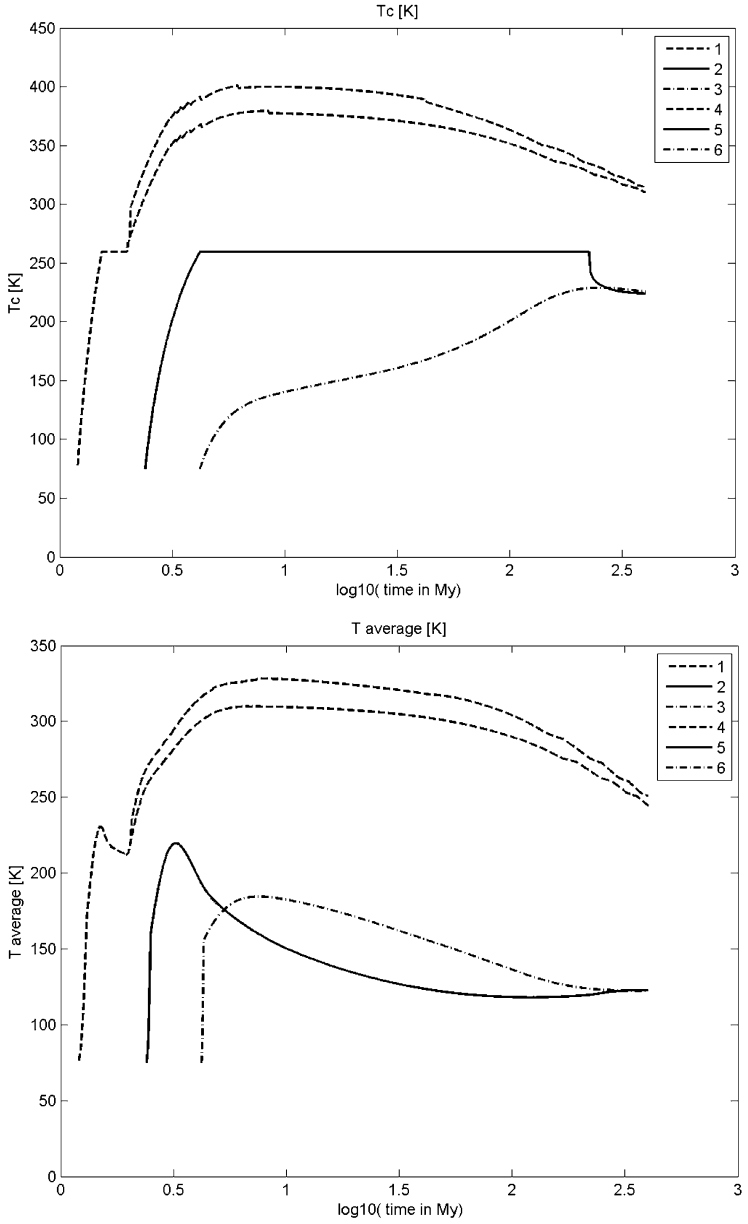

Fig. 8. The role of energy of serpentinization c_{serp} for thermal evolution. Two values of c_{serp} are used: $c_{serp} = 0$ J kg^{-1} (thick lines) and $c_{serp} = 240\,000$ J kg^{-1} (thin lines). Note that lines for $t_{ini} = 2.4$ and 4.2 My overlap indicating that melting and serpentinization do not occur. Other parameters have the "basic" values (see Fig. 4).

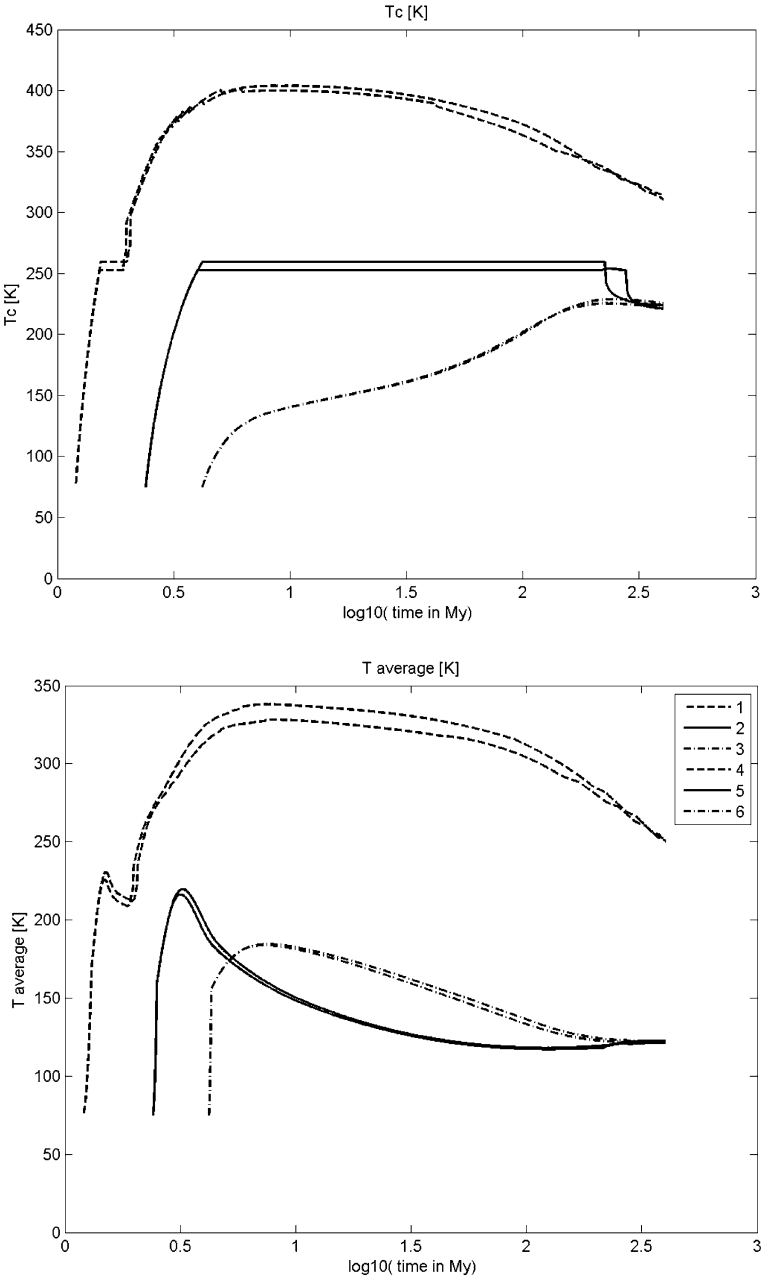

Fig. 9. The role of ammonia content X_{NH3} for thermal evolution. Two values of X_{NH3} are used: $X_{NH3} = 0.1$ (thick lines) and $X_{NH3} = 0$ (thin lines). Other parameters have the 'basic' values as in Fig. 4.

$t_{ini} = 1.2$ My and $X_{NH3} = 0.1$ for time 1.5-2 My, T_c and T_{ave} are below temperatures for the basic model. It is an effect of more intensive cooling by SSC. After 2 My, the melting starts reducing eventually the thickness of mantle and consequently reducing *Ra* for SSC. Lower *Ra* results in a lower cooling intensity and higher temperature. For $t_{ini} = 2.4$ My, when $T_c = T_m$, T_{ave} is slightly increased comparing to the basic model but still melting (and serpentinization) does not occur. For $t_{ini} = 4.2$ there is no visible effect of changed X_{NH3} at all.

5.3 Gravitational differentiation and LSC

Conclusions concerning gravitational differentiation and interaction with LSC are substantially changed in respect to Czechowski (2012) because he used only Stokes formula for the drag force. Here we use also more advanced formulae dependent on the Reynolds number. They are used for processes in Enceladus by Czechowski (2014). We use his approach to Rhea.

The melting allows motion of the silicate grains in the water. The grains' density is higher so negative buoyancy leads them to sink. However, we have also an opposite process, mixing by LSC. Let us consider interaction of these two processes.

The buoyancy force F_g acting on a spherical grain is:

$$F_g = (4/3)\,\pi\, r_g^{\,3}\,(\rho_g - \rho_w)\,g\,, \tag{18}$$

where r_g is the radius of grain, ρ_g is the density of grain, ρ_w is the density of water, and g is the gravity. The drag force F_D acts on the grain moving in fluid. F_D depends on the Reynolds number *Re*. *Re* is given by (*e.g.*, Landau and Lifshitz 1987, Malvern 1969, p. 465):

$$Re = \mathrm{v}\,\rho_w\,L\,/\,\eta_w\,, \tag{19}$$

where η_w is the viscosity of water (~10^{-3} Pa·s), L [m] is the largest dimension of the grain (we use here: $L = 2\,r_g$), v is the velocity of the grain [m·s^{-1}]. We considered two regimes of the flow: high *Re* flow when the drag force for the spherical grain is given by:

$$F_D = \tfrac{1}{2}\,C_D\,S_D\,\rho_w\,\mathrm{v}^2 = \tfrac{1}{2}\,0.45\,\pi\,r_g^{\,2}\,\rho_w\,\mathrm{v}^2 \tag{20}$$

and low *Re* flow when

$$F_D = 6\,\pi\,\eta\,r_g\,\mathrm{v}\,. \tag{21}$$

C_D is a drag coefficient (0.45 for a sphere), while S_D is the area of the cross section [m^2]. Figure 10 presents results of the calculations. We do not know the size of typical grains. The structure of meteorite (*e.g.*, size of chondrules and CAI) suggests grains of the size of 10^{-3} m. Terminal velocity v_{term} of

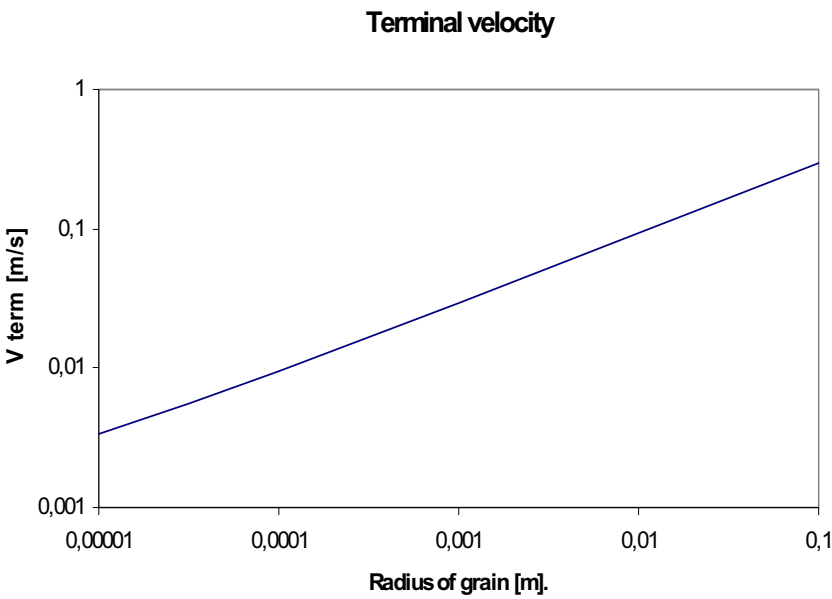

Fig. 10. Terminal velocity v_{term} for different values of radius of the grain r_g for: gravity $g = 0.1$ m s^{-2}, density difference 1500 kg m^{-3}, density of water 1000 kg m^{-3}, and the viscosity 10^{-3} Pa s. Nonlinear drag force given by Eq. 20 is used for high Re (>5), while the Stoke's formula Eq. 21 is used for low Re (<5). The values of terminal velocities presented here should be treated as the upper limits because spherical grains and large gravity are assumed.

such grains is a few cm s^{-1}, if gravity is 0.1 m s^{-2} (close to the center of satellite the gravity is lower than the surface value).

Consider now the interaction of the sinking grains and LSC. The average approximate velocity v_{LSC} of LSC in the molten interior of the satellite is given by the formula obtained from the theory of thermal boundary layer (*e.g.*, Turcotte and Schubert 2002, see also Czechowski 2014, for details):

$$v_{\text{LSC}} = 0.354\ (\kappa/d)\ Ra^{1/2}\,, \tag{22}$$

where the Rayleigh number Ra is given by formula (8). The plot of v_{LSC} is shown in Fig. 11. Note that the velocity of convection v_{LSC} is higher than the terminal velocity v_{term} for considered range of r_g (compare Figs. 10 and 11). It means that differentiation is not possible because the mixing prevails. Czechowski (2014) indicates that even in smaller Enceladus, LSC convection is strong enough for mixing 1 mm grains and consequently not allowing core formation for more than 100 My, *i.e.*, even after decay of the short lived isotopes. It means that the time of core origin depends on the cooling rate of

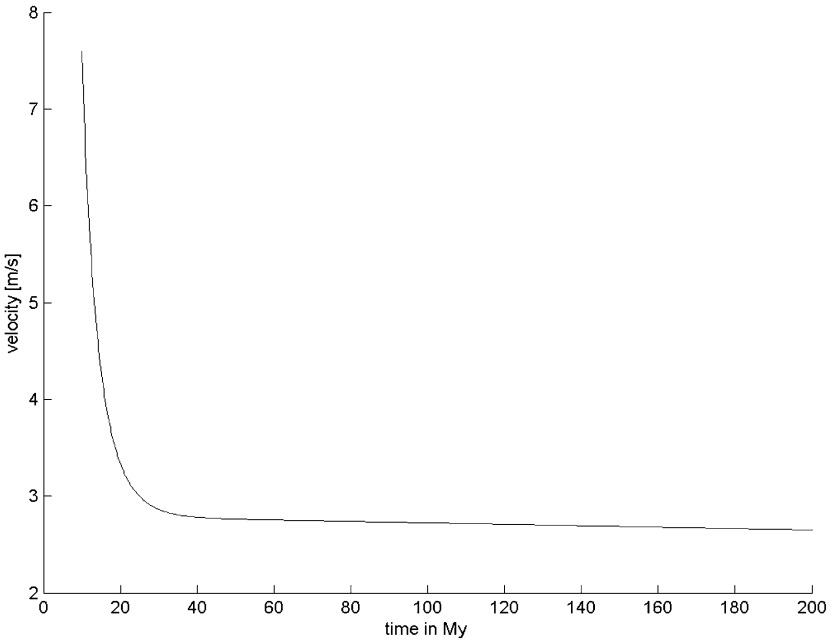

Fig. 11. Velocity of liquid state convection V_{LSC} according to formula 22 *versus* time for $g = 0.1$ m s^{-2}, and $d = 10^5$ m.

the satellite interior. For large Rhea, the bulk of the core is formed only ~200-500 My after CAI. Of course, even during intensive LSC, the largest grains (with high terminal velocity v_{term}) could sink forming a small "proto-core". In this way, LSC segregates the large silicate grains from the small ones.

Czechowski (2014) indicates also that the result of differentiation in Enceladus is a relatively cold core (temperature is close to the melting point of water) of loosely packed grains with water between them (see also Czechowski and Witek 2015). It is permeable for fluids because silicate rocks are permeable up to pressures of above 300 MPa (see discussion in Section 2.2 above). The same conclusion could be applied to Rhea. In fact, the potential temperature for Rhea is lower than for Enceladus (Fig. 3). The pressure in the centre of Rhea is still lower than 300 MPa (Fig. 1).

Temperature increase (above the boiling temperature) resulting from the tidal heating could be a mechanism that removes water from the core in Enceladus. In Rhea, probably there is/was no such mechanism. Eventually, water still could be present between grains and the density of core could be very low. This leads to the conclusion that the gravity data indicating low degree of differentiation could be interpreted also as a full differentiation but

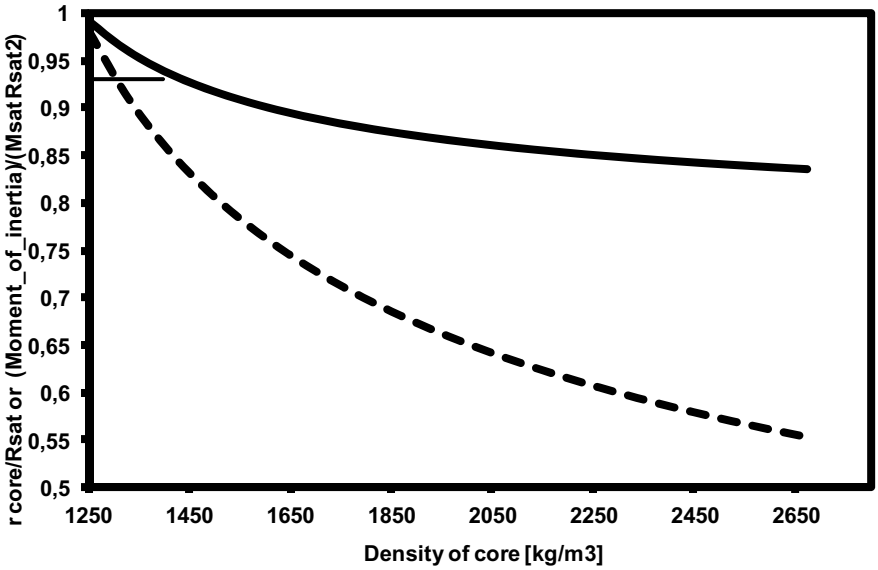

Fig. 12. Some parameters of Rhea as functions of the density of its core. The fully differentiated satellite is assumed for these calculations. Thick solid line – the ratio: (radius of core)/($R_{\rm Sat}$). Dashed line – the ratio: (moment of inertia)/($M_{\rm Sat}R_{\rm Sat}^2$). This ratio for an uniform satellite = 1. The short horizontal solid line shows the ratio (moment of inertia)/($M_{\rm Sat}R_{\rm Sat}^2$) corresponding to the value of this ratio obtained by Iess *et al.* (2007). It intersects the dashed line at ~1300 kg m^{-3}, so the full differentiation of Rhea is possible only if density of the core is ~1300 kg m^{-3}.

the density difference between the undifferentiated mantle and the differentiated porous core is very low (Fig. 12). Unfortunately, we do not know what content of inter-grain water is possible. It depends on the size and shape of the grains and properties of volatiles.

5.4 The role of Coriolis force

The role of Coriolis force for LSC in MIS was suggested already by Czechowski (2012). It could be an important factor determining direction of LSC. The Coriolis force is given by the formula:

$$\boldsymbol{F}_{\rm Cor} = 2\,\rho\,\boldsymbol{v}\times\boldsymbol{\omega}\,, \tag{23}$$

where $\boldsymbol{\omega}$ is the vector of angular velocity of rotation of Rhea. The ratio of Coriolis force $\boldsymbol{F}_{\rm Cor}$ to the viscous term in the Navier-Stokes equation is very large (>3×10^7) even for low spatial scale of the velocity changes, $s = 10^3$ m. The Coriolis force is latitude-dependent, so convection in the molten region

and possible differentiation could also be latitude-dependent. Effects of Coriolis force give a possibility to explain some latitude-dependent features. Czechowski and Leliwa-Kopystynski (2013) use it to explain position of the Iapetus' equatorial ridge and bulge. An equatorial structure is found also on Rhea. According to Schenk *et al.* (2011): "equatorial configuration of Rhea's blue circle is surprisingly similar to that of Iapetus' equatorial ridge (Porco *et al.* 2005, Giese *et al.* 2008)". If the "blue circle" is of endogenic origin then the Coriolis force could be used for explanation of its position.

Note that the very large Prandtl number for SSC makes SSC independent of Coriolis force. However, SSC could be affected by some results of LSC (*e.g.*, by the latitude dependent differentiation). In this sense, SSC could be also latitude-dependent. Latitude-dependent tidal heating was probably never important in Rhea, so its role could be neglected.

5.5 Post differentiation scenarios

Total melting and total differentiation result in a stable situation: the icy mantle of low density overlies the silicate core. Note, however, that after partial differentiation there are 3 spherical regions: (i) the silicate core, (ii) the ice or water layer overlying it, and (iii) the primitive crust. This situation is gravitationally unstable because the density of ice or water is lower than the density of the undifferentiated crust above.

A few possible scenarios after differentiation were proposed – see Czechowski (2012) for more details. All of them lead to presently observed situations, *i.e.*, mostly undifferentiated satellite with the surface covered by depleted ice.

6. CONCLUSIONS AND FUTURE RESEARCH

- The properties of the CI and CM meteorites' matter can be used to estimate the properties of the silicate portion of icy satellites.
- We found that the time of beginning of accretion t_{ini} and the duration of accretion t_{ac} are crucial for the early evolution, especially for differentiation (see Figs. 4 and 7).
- Viscosity of ice close to the melting point η_0, activation energy in formula for viscosity E, and ammonia content X_{NH3} are very important for the evolution, but no dramatic differences are found if realistic values are considered (Figs. 5 and 6).
- The energy of serpentinization c_{serp} is important for the evolution, but its role is also not dominant.
- The LSC operating in the molten part could delay the differentiation and the core formation for a few hundred My.

- The gravity data could be interpreted as showing that Rhea is fully differentiated only if its core has high porosity and low density, ~1300 kg m^{-3}. The result of Anderson and Schubert (2007) allows for such a structure. In fact, there is no mechanism that could remove water from the molten core and the core of Rhea is probably porous. Note also that partial differentiation of a small body is possible only for very narrow time ranges. Moreover, the interpretation of Iess *et al.* (2007) should be reconsidered because of the results of Mackenzie *et al.* (2008) which indicates non-hydrostatic part of Rhea shape.
- LSC could lead to the generation of magnetic field by the planetary dynamo process (*e.g.*, Ivers and Phillips 2012).
- Our results suggest some extensions of the research. Similar models could be developed for other MIS if the gravity field data are provided.
- The role of Coriolis force for MIS should be investigated. It could be responsible for latitude-dependent features like the "blue circle" on the surface of Rhea.

Acknowledgments. This work was partially supported by the National Science Centre (grants 2011/01/B/ST10/06653 and 2013/08/S/ST10/00586). Computer resources of Interdisciplinary Centre for Mathematical and Computational Modeling of Warsaw University are also used in the research. We are very grateful to Dr. Maria Gritsevich and Dr. Daria Kuznetsova for their remarks and suggestions.

References

Abramov, O., and S.J. Mojzsis (2011), Abodes for life in carbonaceous asteroids?, *Icarus* **213**, 1, 273-279, DOI: 10.1016/j.icarus.2011.03.003.

Anderson, J.D., and G. Schubert (2007), Saturn's satellite Rhea is a homogeneous mix of rock and ice, *Geophys. Res. Lett.* **34**, 2, L02202, DOI: 10.1029/2006GL028100.

Barr, A.C., and R.M. Canup (2008), Constraints on gas giant satellite formation from the interior states of partially differentiated satellites, *Icarus* **198**, 1, 163-177, DOI:. 10.1016/j.icarus.2008.07.004.

Bland, P.A., M.D. Jackson, R.F. Coker, B.A. Cohen, B. Webber, M.R. Lee, C.M. Duffy, R.J. Chater, M.G. Ardakani, D.S. McPhail, D.W. McComb, and G.K. Benedix (2009), Why aqueous alteration in asteroids was isochemical: high porosity doesn't equal high permeability, *Earth Planet. Sci. Lett*. **287**, 3-4, 559-568, DOI: 10.1016/j.epsl.2009.09.004.

Brearley, A.J. (2004), Nebular versus parent-body processing. **In:** A.M. Davis, H.D. Holland, and K.K. Turekian (eds.), *Meteorites, Comets, and Planets. Treatise on Geochemistry*, Elsevier-Pergamon, Oxford, 247-268.

Brearley, A.J. (2006), The action of water. **In:** D.S. Lauretta, and H.Y. McSween Jr. (eds.), *Meteorites and the Early Solar System II*, University of Arizona Press, Tuscon, 587-624.

Brearley, A.J., and R.H. Jones (1998), Chondritic meteorites. **In:** J.J. Papike (ed.), *Planetary Materials*, Mineralogical Society of America, Reviews in Mineralogy, Vol. 36, 3-1–3-398.

Canup, R.M., and W.R. Ward (2009), Origin of Europa and the Galilean satellites. **In:** R.T. Pappalardo, W.B. McKinnon, and K. Khurana (eds.), *Europa*, University of Arizona Press in collaboration with Lunar and Planetary Institute, Tucson, 59-83.

Castillo-Rogez, J. (2006), Internal structure of Rhea, *J. Geophys Res*. **111**, E11, E11005, DOI: 10.1029/2004JE002379.

Castillo-Rogez, J., D. Matson, C. Sotin, T. Johnson, J. Lunine, and P. Thomas (2007), Iapetus' geophysics: Rotation rate, shape, and equatorial ridge, *Icarus* **190**, 1, 179-202, DOI: 10.1016/j.icarus.2007.02.018.

Christensen, U. (1984), Convection with pressure and temperature-dependent non-Newtonian rheology, *Geophys. J. Roy. Astr. Soc.* **77**, 2, 343-384, DOI: 10.1111/j.1365-246X.1984.tb01939.x.

Cogoni, M., B. D'Aguanno, L.N. Kuleshova, and D.W.M. Hofmann (2011), A powerful computational crystallography method to study ice polymorphism, *J. Chem. Phys*. **134**, 20, 204506, DOI: 10.1063/1.3593200.

Consolmagno, G.J., and D.T. Britt (1998), The density and porosity of meteorites from the Vatican collection, *Metorit. Planet. Sci.* **33**, 6, 1231-1241, DOI: 10.1111/j.1945-5100.1998.tb01308.x.

Coradini, A., G. Magni, and D. Turrini (2010), From gas to satellitesimals: Disk formation and evolution, *Space Sci. Rev*. **153**, 1, 411-429, DOI: 10.1007/s11214-009-9611-9.

Czechowski, L. (1993), Theoretical approach to mantle convection. **In:** R. Teisseyre L. Czechowski, and J. Leliwa-Kopystyński (eds.), *Dynamics of The Earth's Evolution*, Elsevier, Amsterdam, 161-271.

Czechowski, L. (2006), Parameterized model of convection driven by tidal and radiogenic heating, *Adv. Space Res*. **38**, 4, 788-793, DOI: 10.1016/j.asr.2005.12.013.

Czechowski, L. (2012), Thermal history and large scale differentiation of the Saturn's satellite Rhea, *Acta Geophys*. **60**, 4, 1192-1212, DOI: 10.2478/s11600-012-0041-9.

Czechowski, L. (2014), Some remarks on the early evolution of Enceladus, *Planet. Space Sci.* B. **104**, 185-199, DOI: 10.1016/j.pss.2014.09.010.

Czechowski, L., and K.J. Kossacki (2009), Thermal convection in the porous methane-soaked regolith of Titan: Investigation of stability, *Icarus* **202**, 2, 599-606, DOI: 10.1016/j.icarus.2009.02.032.

Czechowski, L., and K.J. Kossacki (2012), Thermal convection in the porous methane-soaked regolith in Titan: finite amplitude convection, *Icarus* **217**, 1, 130-143, DOI: 10.1016/j.icarus.2011.10.006.

Czechowski, L., and J. Leliwa-Kopystyński (2003), Tidal heating and convection in the medium size icy satellites, *Celest. Mech. Dyn. Astr.* **87**, 1, 157-169, DOI: 10.1023/A:1026136025400.

Czechowski, L., and J. Leliwa-Kopystynski (2013), Remarks on the Iapetus bulge and ridge, *Earth Planet Space* **65**, 8, 929-934, DOI: 10.5047/eps.2012.12.008.

Czechowski, L., and P.P. Witek (2015), Comparison of early evolutions of mimas and enceladus, *Acta Geophys*. **63**, 3, 900-921, DOI: 10.1515/acgeo-2015-0024.

Dalton, J.B., O. Prieto-Ballesteros, J. Kargel, C.S. Jamieson, J. Joliviet, and R. Quinn (2005), Spectral comparison of highly hydrated sulfate salts to disrupted terrains on Europa, *Icarus* **177**, 472-490.

Davaille, A., and C. Jaupart (1993), Transient high-Rayleigh-number thermal convection with large viscosity variations, *J. Fluid Mech*. **253**, 141-166, DOI: 10.1017/S0022112093001740.

Davies, G.F. (2007), Mantle regulation of core cooling: A geodynamo without core radioactivity? *Phys. Earth Planet. In.* **160**, 3-4, 215-229, DOI: 10.1016/j.pepi.2006.11.001.

De Pater, I., and J.J. Lissauer (2001), *Planetary Sciences*, Cambridge University Press, Cambridge, 528 pp.

Desch, S.J., J.C. Cook, T.C. Doggett, and S.B. Porter (2009), Thermal evolution of Kuiper belt objects, with implications for cryovolcanism, *Icarus* **202**, 2, 694-714, DOI: 10.1016/j.icarus.2009.03.009.

Dumoulin, C., M.P. Doin, and L. Fleitout (1999), Heat transport in stagnant lid convection with temperature- and pressure-dependent Newtonian or non-Newtonian rheology, *J. Geophys. Res.* **104**, B6, 12759-12777, DOI: 10.1029/1999JB900110.

Durham, W.B., S.H. Kirby, and L.A. Stern (1998), Rheology of planetary ices. **In:** B. Schmitt, C. de Bergh, and M. Festou (eds.), *Solar System Ices*, Kluwer Academic Publ., Dordrecht, 63-78.

Forni, O., A. Coradini, and C. Federico (1991), Convection and lithospheric strength in dione, an icy satellite of Saturn, *Icarus* **94**, 1, 232-245, DOI: 10.1016/0019-1035(91)90153-K.

Giese, B., T. Denk, G. Neukum, T. Roatsch, P. Helfenstein, P.C. Thomas, E.P. Turtle, A. McEwen, and C.C. Porco (2008), The topography of Iapetus' leading side, *Icarus* **193**, 2, 359-371, DOI: 10.1016/j.icarus.2007.06.005.

Goldsby, D.L., and D.L. Kohlstedt (1997). Grain boundary sliding in fine-grained Ice-I, *Scripta Mater.* **37**, 9, 1399-1405.

Gounelle, M., and M.E. Zolensky (2001), A terrestrial origin for sulphate veins in CI1 carbonaceous chondrites, *Meteorit. Planet. Sci.* **36**, 10, 1321-1329, DOI: 10.1111/j.1945-5100.2001.tb01827.x.

Grasset, O., and P.M. Parmentier (1998), Thermal convection in a volumetrically heated, infinite Prandtl number fluid with strongly temperature-dependent viscosity: Implications for planetary evolution, *J. Geophys. Res*. **103**, B8, 18171-18181, DOI: 10.1029/98JB01492.

Hobbs, P.V. (1974), *Ice Physics*, Oxford University Press, New York.

Hussmann, H., G. Choblet, D.L. Matson, C. Sotin, G. Tobie, and T. van Hoolst (2010), Implications of rotation, orbital states, energy sources, and heat transport for internal processes in icy satellites, *Space Sci. Rev.* **153**, 1-4, 317-348, DOI: 10.1007/s11214-010-9636-0.

Hutchison, R. (2004), *Meteorites: A Petrologic, Chemical and Isotopic Synthesis*, Cambridge University Press, Cambridge, 506 pp.

Iess, L., N.J. Rappaport, P. Tortora, J. Lunine, J.W. Armstrong, S.W. Asmar, L. Somenzi, and F. Zingoni (2007), Gravity field and interior of Rhea from Cassini data analysis, *Icarus* **190**, 2, 585-593, DOI: 10.1016/j.icarus.2007.03.027.

Ivers, D.J., and C.G. Phillips (2012), Anisotropic turbulent thermal diffusion and thermal convection in a rapidly rotating fluid sphere, *Physics Planet. In.* **190**, 1-9, DOI: 10.1016/j.pepi.2011.10.006.

Jaumann, R., R.N. Clark, F. Nimmo, A.R. Hendrix, B.J. Buratti, T. Denk, J.M. Moore, P.M. Schenk, S.J. Ostro, and R. Srama (2009), Icy satellites: Geological evolution and surface processes. **In:** M.K. Dougherty, L.W. Esposito, and S.M. Krimigis (eds.), *Saturn from Cassini-Huygens*, Springer, 637-681, DOI: 10.1007/978-1-4020-9217-6_20.

Jull, A.J.T., S. Cheng, J.L. Gooding, and M.A. Velbel (1988), Rapid growth of magnesium-carbonate weathering products in a stony meteorite from Antarctica, *Science* **242**,4877, 417-419, DOI: 10.1126/science.242.4877.417.

Kargel, J.S., and S. Pozio (1996), The volcanic and tectonic history of Enceladus, *Icarus* **119**, 2, 385-404, DOI: 10.1006/icar.1996.0026.

Kargel, J.S., J.Z. Kaye, J.W. Head, G.M. Marion, and R. Sassen, J.K. Crowley, O. Prieto-Ballesteros, S.A. Grant, and D.L. Hogenboom (2000), Europa's crust and ocean: origin, composition, and the prospects for life, *Icarus* **148**, 1, 226-265, DOI: 10.1006/icar.2000.6471.

Kuskov, O.L., and V.A. Kronrod (2005), Internal structure of Europa and Callisto, *Icarus* **177**, 2, 550-569, DOI: 10.1016/j.icarus.2005.04.014.

Landau, L.D., and E.M. Lifshitz (1987), *Fluid Mechanics*. *Vol. 6*, 2nd ed., Butterworth-Heinemann, 552 pp.

Leliwa-Kopystynski, J., M. Maruyama, and T. Nakajima (2002), The water-ammonia phase diagram up to 300 MPa: Application to icy satellites, *Icarus* **159**, 2, 518-528, DOI: 10.1006/icar.2002.6932.

Llana-Funez, S., K.H. Brodie, E.H. Rutter, and J.C. Arkwright (2007), Experimental dehydration kinetics of serpentinite using pore volumometry, *J. Metamorph. Geol.* **25**, 4, 423-428, DOI: 10.1111/j.1525-1314.2007.00703.x.

Losiak, A., and M.A. Velbel (2011), Evaporite formation during weathering of Antarctic meteorites – A weathering census analysis based on the ANSMET database, *Meteorit. Planet. Sci.* **46**, 3, 443-458, DOI: 10.1111/j.1945-5100.2010.01166.x.

Macke, R.J., G.J. Consolmagno, and D.T. Britt (2011), Density, porosity, and magnetic susceptibility of carbonaceous chondrites, *Meteorit. Planet. Sci.* **46**, 12, 1842-1862, DOI: 10.1111/j.1945-5100.2011.01298.x.

Mackenzie, R.A., L. Iess, P. Tortora, and N.J. Rappaport (2008), A non-hydrostatic Rhea, *Geophys. Res. Lett*. **35**, 5, L05204, DOI: 10.1029/2007GL032898.

Malamud, U., and D. Prialnik (2013), Modeling serpentinization: Applied to the early evolution of Enceladus and Mimas, *Icarus* **225**, 1, 763-774, DOI: 10.1016/j.icarus.2013.04.024.

Malvern, L.E. (1969), *Introduction to the Mechanics of a Continuous Medium*, Prentice-Hall Inc., Englewood Cliffs, 713 pp.

Mangold, N., P. Allemand, P. Duval, Y. Geraud, and P. Thomas (2002), Experimental and theoretical deformation of ice-rock mixtures: Implications on rheology and ice content of Martian permafrost, *Planet. Space Sci*. **50**, 4, 385-401, DOI: 10.1016/S0032-0633(02)00005-3.

Matson, D.L., J.C. Castillo-Rogez, G. Schubert, Ch. Sotin, and W.B. McKinnon (2009), The thermal evolution and internal structure of Saturn's mid-sized icy satellites. **In:** M.K. Dougherty, L.W. Esposito, and S.M. Krimigis (eds.), *Saturn from Cassini-Huygens*, Springer, 577-612, DOI 10.1007/978-1-4020-9217-6_18.

McKinnon, W.B. (1998), Geodynamics of icy satellites. **In:** B. Schmitt, C. de Bergh, and M. Festou (eds.), *Solar System Ices*, Kluwer Academic Publ., Dordrecht, 525-550.

McKinnon, W.B., and M.E. Zolensky (2003), Sulfate content of Europa's ocean and shell: Evolutionary considerations and some geological and astrobiological implications, *Astrobiology* **3**, 4, 879-897, DOI: 10.1089/153110703322736150.

Merk, E., D. Breuer, and T. Spohn (2002), Numerical modeling of ^{26}Al induced radioactive melting of asteroids concerning accretion, *Icarus* **159**, 1, 183-191, DOI: 10.1006/icar.2002.6872.

Mosqueira, I., P. Estrada, and D. Turrini (2010), Planetesimals and satellitesimals: Formation of the satellite systems, *Space Sci. Rev*. **153**, 1, 431-446, DOI: 10.1007/s11214-009-9614-6.

Multhaup, K., and T. Spohn (2007), Stagnant lid convection in the mid-sized icy satellite of Saturn, *Icarus* **186**, 2, 420-435, DOI: 10.1016/j.icarus.2006.09.001.

Opeil, C.P., G.J. Consolmagno, and D.T. Britt (2010), The thermal conductivity of meteorites: New measurements and analysis, *Icarus* **208**, 1, 449-454, DOI: 10.1016/j.icarus.2010.01.021.

Ostro, S.J., R.D. West, M.A. Janssen, R.D. Lorenz, H.A. Zebker, G.J. Black, J.I. Lunine, L.C. Wye, R.M. Lopes-Gautier, S.D. Wall, C. Elachi, L. Roth, S. Hensley, K. Kelleher, G.A. Hamilton, Y. Gim, Y.Z. Anderson, R.A. Boehmer, W.T.K. Johnson, and the Cassini RADAR Team (2006), Cassini RADAR observations of Enceladus, Thethys, Dione, Rhea, Iapetus, Hyperion, and Phoebe, *Icarus* **183**, 2, 479-490, DOI: 10.1016/j.icarus.2006.02.019.

Peacock, S.M. (2001), Are the lower planes of double seismic zones caused by serpentine dehydration in subducting oceanic mantle? *Geology* **29**, 4, 299-302, DOI: 10.1130/0091-7613(2001)029<0299:ATLPOD>2.0.CO;2.

Peltier, W.R., and G.T. Jarvis (1982), Whole mantle convection and the thermal evolution of the Earth, *Phys. Earth Planet. In*. **29**, 3-4, 281-304, DOI: 10.1016/0031-9201(82)90018-8.

Plescia, J.B. (1985), Geology of Rhea. **In:** *Lunar and Planetary Science Conference XVI*, 665-666.

Porco, C.C., E. Baker, J. Barbara, K. Beurle, A. Brahic, J.A. Burns, S. Charnoz, N. Cooper, D.D. Dawson, A.D. Del Genio, T. Denk, L. Dones, U. Dyudina, M.W. Evans, B. Giese, K. Grazier, P. Helfenstein, A.P. Ingersoll, R.A. Jacobson, T.V. Johnson, A. McEwen, C.D. Murray, G. Neukum, W.M. Owen, J. Perry, T. Roatsch, J. Spitale, S. Squyres, P.C. Thomas, M. Tiscareno, E. Turtle, A.R. Vasavada, J. Veverka, R. Wagner, and R. West (2005), Cassini imaging science: Initial results on Phoebe and Iapetus, *Science* **307**, 5713, 1237-1242, DOI: 10.1126/science.1107981.

Porco, C.C., P. Helfenstein, P.C. Thomas, A.P. Ingersoll, J. Wisdom , R. West, G. Neukum, T. Denk, R. Wagner, T. Roatsch, S. Kieffer, E. Turtle, A. McEwen, T.V. Johnson, J. Rathbun, J. Veverka, D. Wilson, J. Perry, J. Spitale, A. Brahic, J.A. Burns, A.D. Delgenio, L. Dones, C.D. Murray, and S. Squyres (2006), Cassini observes the active South Pole of Enceladus, *Science* **311**, 5766, 1393-1401, DOI: 10.1126/science.1123013.

Postberg, F., J. Schmidt, J.K. Hillier, S. Kempf, and R. Srama (2011), A salt-water reservoir as the source of a compositionally stratified plume on Enceladus, Nature **474**, 7353, 620-622, DOI: 10.1038/nature10175.

Prentice, A.J.R. (2006), Saturn's icy moon Rhea: A prediction for its bulk chemical composition and physical structure at the time of the Cassini spacecraft first flyby, *Publ. Astron. Soc. Aust*. **23**, 1, 1-11, DOI: 10.1071/AS05041.

Prialnik, D., and R. Merk (2008), Growth and evolution of small porous icy bodies with an adaptive-grid thermal evolution code. I. Application to Kuiper Belt

objects and Enceladus, *Icarus* **197**, 1, 211-220, DOI: 10.1016/j.icarus.2008.03.024.

Prialnik, D., A. Bar-Nun, and M. Podolak (1987), Radiogenic heating of comets by Al^{26} and implications for their time of formation, *The Astrophys. J.* **319**, 993-1002.

Robuchon, G., G. Choblet, G. Tobie, O. Cadek, C. Sotin, and O. Grasset (2010), Coupling of thermal evolution and despinning of early Iapetus, *Icarus* **207**, 2, 959-971, DOI: 10.1016/j.icarus.2009.12.002.

Roscoe, R. (1952), The viscosity of suspensions of rigid spheres, *Brit. J. Appl. Phys*. **3**, 8, 267-269.

Rothery, D.A. (1992), *Satellites of the Outer Planets*, Clarendon Press, Oxford.

Rubin, A.E., J.M. Trigo-Rodrıguez, H. Huber, and J.T. Wasson (2007), Progressive alteration of CM carbonaceous chondrites, *Geochem. Cosmochim. Acta* **71**, 9, 2361-2382, DOI: 10.1016/j.gca.2007.02.008.

Rutter, E.H., S. Llana-Funez, and K.H. Brodie (2009), Dehydration and deformation of intact cylinders of serpentinite, *J. Struct. Geol.* **31**, 1, 29-43, DOI: 10.1016/j.jsg.2008.09.008.

Schenk, P., D.P. Hamilton, R.E. Johnson, W.B. McKinnon, C. Paranicas, J. Schmidt, and M.R. Showalter (2011), Plasma, plumes and rings: Saturn system dynamics as recorded in global color patterns on its midsize icy satellites, *Icarus* **211**, 1, 740-757, DOI: 10.1016/j.icarus.2010.08.016.

Schubert, G., T. Spohn, and R.T. Reynolds (1986), Thermal histories, compositions and internal structures of the moons of the solar system. **In:** J.A. Burns and M.S. Matthews (eds.), *Satellites*, The University of Arizona Press, Tucson, 224-292.

Schubert, G., D.L. Turcotte, and P. Olson (eds.) (2001), *Mantle Convection in the Earth and Planets*, Cambridge University Press, Cambridge, 940 pp., DOI: 10.1017/CBO9780511612879.

Schubert, G., J.D. Anderson, B.J. Travis, and J. Palguta (2007), Enceladus: Present internal structure and differentiation by early and long-term radiogenic heating, *Icarus* **188**, 2, 345-355, DOI: 10.1016/j.icarus.2006.12.012.

Schubert, G., H. Hussmann, V. Lainey, D.L. Matson, W.B. McKinnon, F. Sohl, C. Sotin, G. Tobie, D. Turrini, and T. Van Hoolst (2010), Evolution of icy satellites, *Space Sci. Rev*. **153**, 1, 447-484, DOI: 10.1007/s11214-010-9635-1.

Sharpe, H.N., and W.R. Peltier (1978), Parameterized mantle convection and the Earth's thermal history, *Geophys. Res. Lett*. **5**, 9, 737-740, DOI: 10.1029/GL005i009p00737.

Showman, A.P., and R. Malhotra (1999), The Galilean satellites, *Science* **286**, 5437, 77-84, DOI: 10.1126/science.286.5437.77.

Sinha, M., and R. Evans (2004), Mid-ocean ridges: Hydrothermal interactions between the lithosphere and oceans. **In:** C.R. German, J. Lin, L.M. Parson

(eds.), *Mid-Ocean Ridges: Hydrothermal Interactions Between the Lithosphere and Oceans*, AGU Press, Washington, 19-62.

Sohl, F., T. Spohn, D. Breuer, and K. Nagel (2002), Implications from Galileo observations on the interior structure and chemistry of the Galilean satellites, *Icarus* **157**, 1, 104-119, DOI: 10.1006/icar.2002.6828.

Sohl, F., M. Choukroun, J. Kargel, J. Kimura, R. Pappalardo, S. Vance, and M. Zolotov (2010), Subsurface water oceans on icy satellites: Chemical composition and exchange processes, *Space Sci. Rev*. **153**, 1-4, 485-510, DOI: 10.1007/s11214-010-9646-y.

Solomatov, V.S. (1995), Scaling of temperature- and stress-dependent viscosity convection, *Phys. Fluids* **7**, 2, 266-274, DOI: 10.1063/1.868624.

Stein, C., S. Stein, and A. Pelayo (1995), Heat flow and hydrothermal circulation. **In:** S.E. Humphris, R.A. Zierenberg, L.S. Mullineaux, and R.E. Thomson (eds.), *Seafloor Hydrothermal Systems*, American Geophysical Union, Washington, D.C., 425-445, DOI: 10.1029/GM091p0425.

Tomeoka, K., and P.R. Buseck (1988), Matrix mineralogy of the Orgueil CI carbonaceous chondrite, *Geochim. Cosmochim. Ac*. **52**, 6, 1627-1640, DOI: 10.1016/0016-7037(88)90231-1.

Travis, B.J., J. Palguta, and G. Schhubert (2012), A whole-moon thermal history model of Europa: Impact of hydrothermal circulation and salt transport, *Icarus* **218**, 2, 1006-1019, DOI: 10.1016/j.icarus.2012.02.008.

Turcotte, D.L., and G. Schubert (eds.) (2002). *Geodynamics*, 2nd ed., Cambridge University Press, Cambridge, 450 pp.

Vance, S., J. Harnmeijer, J. Kimura, H. Hussmann, B. DeMartin, and J.M. Brown (2007), Hydrothermal systems in small ocean planets, *Astrobiology* **7**, 6, 987-1005, DOI: 10.1089/ast.2007.0075.

Velbel, M.A., D.T. Long, and J.L. Gooding (1991), Terrestrial weathering of Antarctic stone meteorites: Formation of Mg-carbonates on ordinary chondrites, *Geochim. Cosmochim. Ac.* **55**, 1, 67-76, DOI: 10.1016/0016-7037 (91)90400-Y.

Velbel, M.A., E.K. Tonui, and M.E. Zolensky (2012), Replacement of olivine by serpentine in the carbonaceous chondrite Nogoya (CM2), *Geochim. Cosmochim. Ac.* **87**, 117-135, DOI: 10.1016/j.gca.2012.03.016.

Walsh, J.B., and W.E. Brice (1984), The effect of pressure on porosity and the transport properties of rock, *J. Geophys. Res*. **89**, NB11, 9425-9432, DOI: 10.1029/JB089iB11p09425.

Weisberg, M.K., T.J. McCoy, and A.N. Krot (2006), Systematics and evaluation of meteorite classification. **In:** D.S. Lauretta and H.Y. McSween Jr. (eds.), *Meteorites and the Early Solar System II*, University of Arizona Press, Tuscon, 19-52.

Young, E.D., K.K. Zhang, and G. Schubert (2003), Conditions for pore water convection within carbonaceous chondrite parent bodies — implications for

planetesimal size and heat production, *Earth Planet. Sci. Lett*. **213**, 3-4, 249-259, DOI: 10.1016/S0012-821X(03)00345-5.

Zolotov, M.Y. (2007), An oceanic composition on early and today's Enceladus, *Geophys. Res. Lett.* **34**, 23, L23203, DOI: 10.1029/2007GL031234.

Zolotov, M.Y., and M.V. Mironenko (2007), Hydrogen chloride as a source of acid fluids in parent bodies of chondrites. **In:** *38th Lunar and Planetary Science Conference*, Abstract #2340.

Zolotov, M.Y., and E.L. Shock (2001), Composition and stability of salts on the surface of Europa and their oceanic origin, *J. Geophys. Res*. **106**, E12, 32815-32827, DOI: 10.1029/2000JE001413.

Received 2 July 2015
Received in revised form 17 November 2015
Accepted 22 January 2016